UNIL | Université de Lausanne
Faculté des géosciences
et de l'environnement

Master of Science in Environmental Science

Biofilm structure shaped by porous media flow

Tanja Orsatti

Under the direction of Pietro De Anna
And Dr. David Scheidweiler

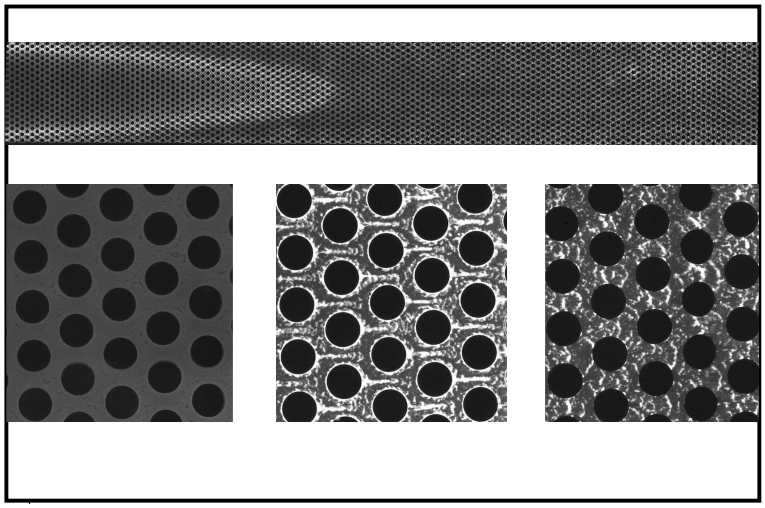

January 2023

UNIL | Université de Lausanne

Information importante: Le texte de ce travail n'a pas été rédigé en vue d'une publication ou dans l'optique d'une édition ou diffusion ; son format et tout ou partie de son contenu répondent donc à cet état de fait. Les contenus n'engagent pas l'Université de Lausanne.
Ce texte n'en est pas moins soumis aux règles et droits usuels sur les droits d'auteur. A ce titre, les citations tirées du présent mémoire ne sont autorisées que dans la mesure où la source et le nom de l'auteur.e sont clairement cités. La loi fédérale sur le droit d'auteur et les droits voisins (LDA) est en outre applicable.

Convention de transmission des travaux de master en Sciences de l'Environnement déposés dans les archives de la Bibliothèque des Sciences de la Terre

Les travaux de masters en Sciences de l'Environnement sont juridiquement considérés comme des copies d'examen et sont, à ce titre, confidentiels.

Cependant, la confidentialité peut être exceptionnellement levée avec l'accord de l'auteur du travail de master et du directeur du travail de master pour des **motifs de recherche scientifique**, **sans but commercial**.

- Par sa signature, l'auteur du travail de master en autorise la transmission sous format papier et électronique pour des motifs de recherche scientifique, par la bibliothèque des Sciences de la Terre.
- Le directeur du travail doit indiquer si le travail contient des données juridiquement confidentielles (par ex. des données de compagnies pétrolières ou minières) ne pouvant pas être diffusées.
- Le directeur du travail peut en outre décider d'une période d'embargo durant laquelle le travail ne sera pas transmis, même pour des motifs de recherche scientifique. La période d'embargo s'éteint automatiquement au plus tard à la retraite du directeur du travail ou lorsque le directeur quitte l'université de Lausanne.

Titre du travail : Biofilm structure shaped by porous media flow

Auteur : Tanja Orsatti Directeur : Pietro de Anna

J'autorise la transmission de mon travail de master pour des motifs de recherche scientifique sans but commercial.

Lausanne, le……., signature de l'étudiant

Le travail contient des données confidentielles et ne peut pas être transmis oui / non

Le travail est soumis à un embargo jusqu'au ……..…. (date)

L'embargo peut être levé avant la date indiquée moyennant mon accord oui / non

Lausanne, le ……., signature du directeur

Résumé

Les roches souterraines sont des réservoirs d'eau très importants, l'eau peut s'écouler à travers des milieux saturés poreux ou fracturés dans lesquels les composés peuvent être transportés passivement avec l'eau. Dans l'espace poreux, des processus de mélange et de transport ont lieu et contrôlent les réactions chimiques et biologiques, comme la croissance des biofilms. La croissance et le transport des biofilms sont classiquement étudiés à travers la théorie CFT (théorie de la filtration colloïdale) sans considérer les processus physiques et biologiques liés aux cellules microbiennes, leur métabolisme et leur division.

Le transport des micro-organismes, dans cette étude des bactéries et des biofilms, est plus complexe que le transport colloïdal, car ils interagissent avec la structure et entre eux. Des recherches récentes ont montré que les bactéries transportées à travers des milieux poreux s'organisent en différentes structures et de manière hétérogène. Deux structures sont généralement observées : les streamers et le base biofilm, et selon les études, ces structures apparaissent en fonction du débit et des nutriments. Cependant, les recherches récentes ont conclu que le transport par biofilm reste un domaine ouvert avec de nombreuses inconnues, par exemple, il n'a pas été compris si la croissance de la biomasse totale dans un milieu poreux suit un modèle logistique et aussi de quoi dépend la différenciation structurelle du biofilm.

Grâce à des techniques récemment développées telles que la microfluidique et la possibilité de mener des expériences sur de longues périodes de temps et d'acquérir des images en temps différé, il a été possible d'analyser la croissance et la dispersion des biofilms à travers un milieu poreux. La dispersion de la biomasse a été analysée à l'échelle macroscopique mais aussi à l'échelle des pores, de sorte qu'il a été possible d'avoire une idée générale à toutes les échelles du comportement des biofilms dans certaines conditions. Après une série d'expériences utilisant deux stratégies différentes de croissance de la bactérie *P.Putida* (KT2440 ΔfliM) au travers de milieux poreux sous un flux contrôlé dans un espace confiné, et après des analyses qualitatives et quantitatives, il a été conclu que la biomasse totale ne croît pas selon le modèle logistique et que les structures au sein d'un milieu poreux se développent de manière hétérogène en fonction des conditions initiales et des substances injectées dans le système.

Abstract

Underground rocks are really important water reservoir, water can flows trough porous or fractured saturated media within which compounds can be passively transported with water. In the pore space mixing and transport process takes place and controls chemical and biological reactions, as biofilm growth. Biofilm growth and transport is classically studied trough the CFT theory (colloid filtration theory) without consider the physical and biological process relies to the microbial cells and their metabolism and division.

Transport of microorganism, in this study of biofilm, is more complex as the colloid transport, as they interact with the structure and between themselves. Recent research has shown that bacteria transported through porous media organise themselves into different structures and in a heterogeneous way. Two structures are generally observed: streamers and base biofilm, and according to studies these structures occur as a function of flow and nutrients. However, recent research has concluded that biofilm transport is still an open field with many unknowns, e.g. it has not been understood whether the growth of total biomass in a porous media follows a logistic model and also what the structural differentiation of the biofilm depends on.

Thanks to recently developed techniques such as microfluidics and the possibility of conducting experiments over long time periods and acquiring time lapsed images, it was possible to analyse the growth and dispersion of biofilms through a porous media. Biomass dispersion was analysed at the macroscopic scale but also at the pore scale, so that it was possible to get a general idea at all scales of how biofilms behave under certain conditions. After a series of experiments using two different strategies of growth of *P.Putida* bacteria (KT2440 ΔfliM) trough porous media under a controlled flow in a confined space, and after qualitative and quantitative analyses, it was concluded that the total biomass does not grow according to the logistic model and that the structures within a porous media develop in an heterogeneous way depending by the initial conditions and by the substances injected into the system.

Contents

Chapter 1

Introduction

1.1 The underground as highly reactive zone

The underground is a highly reactive zone in the sense that it serves as a water and nutrients reservoir for the plethora of organisms living there, whose metabolic activity control the production of new soil [1]. The underground top layer is the soil, the superficial part of our Earth. It is the substrate for natural vegetation and cultivated plants: a repository of unique and essential raw material supporting the life of a broad multitude of living organisms. As mentioned above, one of the underground functions is to be a main water reservoir. This is why we speak of the underground as an highly reactive zone [1]. In fact, when rainwater reaches the Earth surface, it will move by three main processes: evaporation, surface flow and infiltration. The latter, infiltration, is the transfer of water through the surface layers of the soil towards the deeper underground. The infiltrating water initially finds a dry soil: therefore, in the surface layer there is either air or water (unsaturated zone), up to the zone where the pressure is so high that the air is expelled from the pores (saturated zone). The layer between the unsaturated and the saturated zone is called the water, this is why aquifers are confined zones. Below the soil top layer, are the aquifers: natural geological structures composed by a layer of permeable rock or unconsolidated material which is saturated with water so that the whole system is sufficiently conductive to allow a significant groundwater flow.

Within aquifers, water can flow through different types of structures that are typically divided into two large groups: fractured or porous. The first kind of structures are typically low in permeability and composed of consolidated rocks that have undergone fracturing due to natural or induced stresses (i.e. seismic phenomena or fracking process). In contrast, porous media are permeable and typically unconsolidated materials that allow water to move through solid and impermeable grains that separate spaces, the pores, that are filled by water [2]. Natural flowing water is rarely

pure, but it is rather rich in other compounds (which can be suspended or dissolved), that can be inert, thus passively transported, or can interact with the other compounds or with the solid medium matrix. It is within the pore space that transport and mixing of such compounds take place, controlling the complex dynamics of chemical and biological reaction rates [3], such as dissolution and precipitation [4], ion exchange [4], bio-mineralization [5] and finally biofilm growth [6].

Reactive transport in geologic media is often described in terms of classical macro-dispersion theories that assume compounds concentrations to be well mixed at some pre-defined scale. The dispersion coefficients used to fit measured data depend on the observation scale (e.g. [7]) and indicate spreading of a compound rather than the mixing degree (e.g. [8]).

These classical models are often used to describe also situations in which transported substances are not well mixed. However, it is important to note that in many realistic scenarios, transported substances (solutions or suspensions) are not well mixed within the pores. This plays a key role in controlling larger scale, macroscopic, mixing-driven processes, like reactions or microbial activity, as observed in a range of natural systems, from turbulent and chaotic flows (e.g. [3]) to transport in porous and fractured media (e.g. [9]).

In particular, when bacterial colonies are confined within the tiny volumes of pores, the individual cells cannot physically access resources and use them for their metabolic activities. In such conditions, classical models describing microbial growth that are based on well-mixed assumption (all cells have the same access to the same amount of resources) fail to represent the overall biomass growth and, thus, likely also metabolic-driven phenomena.

1.2 Underground porous structure, fluid flow and transport

Medium structure

Most natural environment are characterized by a porous structure hosting fluids whose displacement (usually driven by a pressure drop) is controlled by the size, shape and organization of the pores themselves [2].

Aquifers, the subsurface groundwater reservoirs, can be defined as *any significant volume of subsurface which containing saturated material to retains a significant quantities of water* [1] that can be transmitted when subject to a pressure drop. There are many medium structural properties controlling the way water can flow through them, let's analyse the principal ones.

The medium porosity, ϕ, is defined as the ratio between the volume of all pores (V_p) and the total medium volume (V_{tot}):

$$\phi = \frac{V_p}{V_{tot}}. \tag{1.1}$$

It measures the capacity of a medium to host fluids. Values for porosity can vary a lot [10, 1]: for non consolidated sediments ϕ varies for sand and gravel in the range 25% - 40%, for clay it ranges between 40% and 70%, while for consolidated rocks it varies from crystalline rock (0% - 10%) to dolomite limestone (0% - 20%) or karstic limestone and fractured basalt (5% - 50%) [11].

The size of the pore also is very important since it represent the size of the opening through which fluids are forced to pass and, due to their finite viscosity, the smaller the pore size, the more energy they need to move through them [2]. Typically, pores size ranges from 10^{-6} to 10^{-1} m [2]. On top of the pore size, also the pore/grains geometrical organization can play a key role. Generally, the more the rocks geometry is heterogeneous and the variability of grains size is broad, the smaller the porosity of the system will be (since small and fine grains can fill the space between the larger ones) [10]. In realistic scenarios, the grains can also be permeable to fluids and, thus begin characterized by a porosity, said secondary porosity, but the size of the openings within the grains is so small that it does not affect the total medium permeability. While for homogeneous media the average grain or pore size is often enough to describe the overall structure, for heterogeneous media a statistical description of the medium structure is often provided in terms of the grain/pore size, the Probability Density Function [12].

Fluid flow

Due to hydraulic gradients (pressure drops), water flows within aquifers squeezing among pores. The connection between the average fluid velocity q and the overall macroscopic hydraulic gradient ∇h is described by the Darcy's law:

$$q = -K \nabla h, \tag{1.2}$$

The ability of the geological medium to host fluid flow is summarized in the value of the hydraulic conductivity K in eq. (1.2), that has units of a velocity, thus [m/s], representing the velocity of a fluid moving through a porous system under the action of a unitary hydraulic gradient. The hydraulic conductivity depends on the medium structural properties and also on the fluid density ρ and viscosity μ [2].

The fluid dynamic viscosity (μ, $[N/\frac{s}{m^2}]$) quantifies the fluid resistance to shear. The origin of shear stress is related to the inter-molecular interaction that are bounded to one another so that each molecule moving drag the ones that are close to it and vice-versa. While moving with the flow, since shear stress τ is directly proportional to velocity spatial variation

$$\tau = \mu \frac{dv}{dy}, \tag{1.3}$$

and within each pore the fluid velocity profile, like in a pipe, has a parabolic shape, the shear stress is higher near the grains and it is zeros in the middle of the pore [1]. As defined in eq. (1.3), the constant of proportionality between shear stress and velocity gradient is the dynamic viscosity μ. Often it is considered the ratio of dynamic viscosity and fluid density, also known as fluid kinematic viscosity (ν, $[m^2/s]$) defined as:

$$\nu = \frac{\mu}{\rho}. \tag{1.4}$$

The flow regime depends on the overall pressure gradient, thus the average velocity, but also on the fluid viscosity, density and characteristic distance λ over which the fluid velocity varies. Flow can be turbulent, chaotic or laminar, depending on the relative importance of viscous and intertinal forces in controlling the fluid movement. The adimensional quantity representing the ratio of intertial to viscous forces is the Reynolds number, R_e, defined as:

$$R_e = \frac{\rho\, q\, \lambda}{\mu} = \frac{q\, \lambda}{\nu} \tag{1.5}$$

For Re number values below unity, viscosity dominates the fluid motion that is stationary (time independent) and laminar. For higher values of Re, typically $0 < Re < 2000$ the fluid motion is hard to precidt and temporally variable and the flow regime is said chaotic. For even higher values, $Re > 2000$ eddies and vortexes emerge leading to the complex phenomenon of turbulence [2].

As mentioned earlier, subsurface environment, like aquifers, are composed of porous materials within which groundwater can move within pores of characteristic size often below 1 mm with velocities of the order of 1 m/d$\sim 20\,\mu$m/s. Considering the viscosity of water ($\nu = 1$ mm^2/s) the Reynolds number for such a flowing system is below unity and flow typically laminar.

The spatial and temporal fluid velocity $\vec{u}$ distribution is obtained by imposing momentum conservation, that is mathematically expressed by the well known Navier-Stokes equations and their boundary consitions, representing the no-slip at every solid surface (i.e. fluid molecules in contact

with the solid surfaces get attached and do not move, while the other can flow) [1, 2]. The Navier-Stokes equations, can be simplified when intertia can be neglected, or for low Reynolds numbers (Re <1). For a horizontal system, ignoring gravity, we get:

$$\nabla p = -\mu \nabla^2 \vec{u} \tag{1.6}$$

where p is the fluid pressure. As mentioned before, the single pore flow is the same as the pipe of radius R flow [12] described by the Hagen-Poiseuile law, from which we get the velocity variation at the distance r from the pore (or pipe) center:

$$u(r) = \frac{\nabla p}{4\mu}(R^2 - r^2), \tag{1.7}$$

it predict a parabolic velocity profile that is maximum at the pore center, and it smoothly reduces down to zero getting closer to the grain.

Given a porous system porosity and average pore size it is possible to link them directly to the system hydraulic conductivity K for simple and homogeneous medium composed of spheres of identical diameter d_g and porosity ϕ. Assuming that the overall fluid flow is equivalent to the one moving through a set of parallel pipes of effective diameter d and imposing that the overall viscous friction, due to drag exerted by the solid medium surfaces on the fluid is the same in both cases (porous system and pipes) it is possible to derive the value for d. Since for a pipe the exact relationship between fluid velocity, pipe diameter, fluid density and viscosity is known (Hagen-Poiseuille flow), with some geometrical argument on the volume-to-surface ratio, it is possible to compute the effective diameter of the pipes to get the same friction as in the homogeneous porous system. Kozeny-Carman derived this that can be expressed in therms of the formula carrying their names:

$$q = -\frac{d_g^2}{180}\frac{\phi^3}{(1-\phi)^2}\frac{\rho g}{\mu}\nabla h \tag{1.8}$$

where g is the value of gravitational acceleration. This expression can be re-written as:

$$q = -\frac{k}{\mu}\nabla p \tag{1.9}$$

where it has been introduced the medium intrinsic permeability k that contains only the medium structural properties and do not depends on the fluid ones.

Transport phenomena

Dispersion through a porous medium is the macroscopic phenomenon that increase the longitudinal spatial occupancy of the transported substance. Dispersion is controlled by two processes: advection (displacement by fluid flow) and molecular diffusion (associated to thermal agitation). Diffusion is the mechanism according to which a substance is spreading isotropically (in the same way along all directions) through the fluid by the random motion its own particles. It is influenced by the interactions with fluid particles and with solid obstacles (like grains). The description of the diffusion process can be expressed in terms of the two Fick's laws. The first law of Fick states that the diffusive mass flux is proportional to the local concentration gradient:

$$\vec{J} = -D_m \nabla c \tag{1.10}$$

where D_m is the diffusion coefficient and ∇c is the substance concentration gradient. The negative sign implies that mass moves from higher to lower concentrations. The second law of Fick represents mass conservation:

$$\frac{\partial c}{\partial t} = -\nabla \cdot \vec{J}. \tag{1.11}$$

If a there is a temporal variation of the local substance concentration (mass) this must be balanced by an equivalent spatial variation of the mass flux. Combining these two laws we get:

$$\frac{\partial c}{\partial t} = D_m \nabla^2 c. \tag{1.12}$$

which is a partial differential equation, known as diffusion equation, describing the spatio-temporal variation of a substance due to molecular diffusion.

Advection is the transport of a substance by the fluid displacement. Such transport can be described in terms of mass conservation, eq. (1.11), for which the advective mass flux is:

$$\vec{J} = \vec{u}\, c \tag{1.13}$$

proportional to the product between the transported substance concentration and the local fluid velocity.

Combining the advective and diffusive mass fluxes withinthe mass conservartion equation, we can

derive the so-called Advection-Diffusion Equation, ADE, describing the transport of a substance:

$$\frac{\partial c}{\partial t} = -\vec{u}\nabla c + D\nabla^2 c. \tag{1.14}$$

The substance concentration c and fluid velocity $\vec{u}$ are both function of the three dimensional space $\vec{x}$. Unfortunately, in most configurations and realistic conditions, it is not possible to know the velocity field value at each spatial locations and compute the substance transport analytically. Numerical computation can be used but computing the transport of a substance resolving a medium from the smallest pore size of a few microns up the overall medium size of several meters, or more, is practically not possible. Thus, the description of the transport phenomenon is often simplified by considering the averaged concentration longitudinal profile $\bar{c}(x,t)$, where x represent the unidimensional distance from the system inlet where space has been discretized with bins of size much larger than the average pore size. Then, the previous ADE eq. (1.14) is substituted with a similar one:

$$\frac{\partial \bar{c}}{\partial t} = -q\,\nabla\bar{c} + D^*\nabla^2\bar{c}. \tag{1.15}$$

where the diffusion coefficient has been replaced by the macroscopic dispersion coefficient D^* and the local fluid velocity by the average Darcy velocity q. The previous equation is called Advection-Dispersion-Equation [2]. and it describes transport under homogeneous flow conditions. It is used also to model and predict transport of microbial cells without taking into account their metabolic activities [13, 14].

1.3 Microbial life in the subsurface

Bacteria are unicellular prokaryotic microorganisms (a domain of simple living beings characterized by cells without a nucleus) that are independent of other cells, unlike plants and animals that are unable to survive in nature without being part of multi-cellular systems [5]. Bacteria, in particular, get a lot of attention from microbiology as they have very important practical effects. In a general way, micro-organisms have an influence on all other forms of life (humans, animals, plants) and in all environments (water, soil, ...), which is why microbiology is one of the most important biological sciences [5]. It can be said that the cell is the fundamental unit of life: each individual, to be isolated, is surrounded by a lipid membrane that defines them as selectively permeable to exchanges of material with the external environment. Such exchanges allow cells to have most of characteristics common to all organisms, namely metabolism, growth, evolution, motility, differentiation and communication [5]: the first three are found in all the cells, while the others three only in some cells.

From a physical standpoint, individual bacteria may act as colloidal particles in suspension within a liquid as water and can be transported by its flow. As for colloids, when bacterial cells are transported near a solid surface there is a force attracting them near it and makes them deposit, but sedimentation has importance only when there is an aggregation of bacteria creating a microbial community called biofilm [15].

Bacteria have two natural ways to grow as colonies by cell division: as *planktonic* cells or organized into *biofilms*. The first is a life phase as unicellular elements in which cells are free to float and move while suspended and transported by the flow. The case of biofilm is a multi-cellular phase, where cells aggregate in *sessile* colonies living close to each other [16]. In nature the biofilm dominate over plantkonic cells. Biofilm is the ensemble of microbial cells and cell-secreted extracellular polymeric substance (called EPS). EPS protect biofilm cells from hard environmental conditions and from antibiotics, favoring their proliferation [17, 18]. Biofilm formation can be divided in three principal phases: at first, the attachment phase between cells and a solid surface, then, the growth by cell division into active sessile colonies and, finally, the release phase allowing individual cells to explore the environment in planktonic phase [16].

It can therefore be said that the biofilm formation is cyclical, initially with single cells living separately, then aggregating in the form of sessile communities and finally detaching and starting a new life cycle. Similarly, one can also say that the growth of bacteria is cyclical, but following a logistic model: in fact, the biomass increases until it reaches a maximum and then decreases until, if conditions are favorable, growth resumes. In the following chapter, the microbial growth cycle is better described.

Microbial growth: logistic model

To study the growth of a microbial community, the classical diagnostic quantity to be tracked is simply the overall population size that can be expressed in terms of mass (in g) or in cells number or in terms of the initial population size. As previously mentioned, due to their metabolic activity, cells are able to uptake nutrients from the external environment to transform them into new biomass and, eventually, new cells. Through the division mechanism each cell, called mother, can divide into two cells, called daughters, replicating identically its own genetic material. The simplest mathematical model that can represent the overall population growth by cell division can be set as follows. Every t_g the number of new cells produced by the division mechanism is identical to the actual population,

thus the population size N (i.e. the number of cells composing the community) undergoes:

$$\frac{dN}{dt} = N(t), \tag{1.16}$$

where the generation time t_g represents interval between two division events. In realistic scenarios at each time there is a fraction k of the population that actually divide, while the rest of the cells are uptaking nutrients, spending energy on other metabolic activities etc... Thus, a more realistic model to represent the overall population growth would be

$$\frac{dN}{dt} = k\,N(t), \tag{1.17}$$

The rate k at which the population divide vary depending on the environmental conditions (presence of nutrients, temperature, available space ...) but also on incubation conditions. Such rate, k, can vary from $1/\text{min}$ up to $1/\text{d}$ [5]. The solution of the two previous ordinary differential equations is exponential and it represents an early stage real population growth: the overall cells division rate (dN/dt) is initially very low but quickly increases as the population: thus, while initially the growth is not really influenced by the nutrients or space availability, at later times the more cells are produced, the less nutrients and space will be available and, thus, the growth rate must decrease. To take that into consideration, the model eq. (1.17) can be modified as follows:

$$\frac{dN}{dt} = k\,N(t) - \frac{k\,N(t)^2}{N_\infty} = k\,N(t)\,\left(1 - \frac{N(t)}{N_\infty}\right) \tag{1.18}$$

with N_∞ is the maximum number of cells that the whole system (with a given amount of nutrient and space available) can sustain, it is the so-called system *carrying capacity*. According to the mass action law, the term proportional to the population size squared ($N(t)^2$) represents the probability of cells to physically meet and, thus, represents the spatial occupancy of the population that when becomes too large, compared to the system carrying capacity, slows down the overall growth. The mathematical model expressed by eq. (1.18) is called *logistic model*.

The population exponential growth is not sustainable over time due to limiting factors such as nutrients, space, oxygen availability that are all lumped into the single parameter N_∞. Actual experiments confirm the prediction of the logistic model and, in particular, four growth phases are observed [5]: an initial **lag phase** followed by the **exponential phase** leading to a **stationary phase** and, finally, a **death phase** (not actually predicted by the model above) in which cells consumed all the available nutrients and die, as showed in figure 1.1.

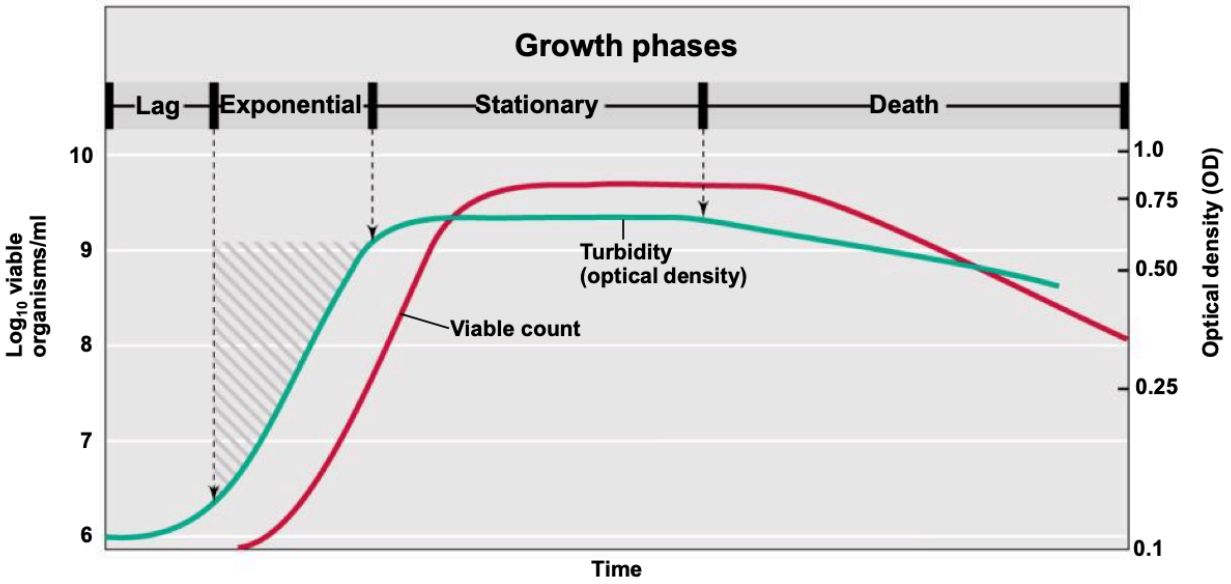

Figure 1.1: Microbial logistic model: in red is represented the cells growth in the culture which are capable of reproducing, in green the optical density (light scattering by a culture) [5].

The **lag phase** is the period needed by cells to adjust to their environment and begin the cell division process: in fact from the moment cells are inoculated into a new medium to the moment when exponential growth begins there is a phase where the cells have to adapt to the new environment, uptake nutrients and begin biosynthesis. In addition, heat or radiation shocks can also create damage to the cells and therefore need a period to stabilize, for example due to transfer of culture from Petri dish to liquid. Moreover, culture media changes maybe also the useful to microbial cells to develop the new enzymes [5]. Once the cells have stabilized themselves in the new culture environment, they are able to start cell division and thus the **exponential phase** of growth. As already briefly mentioned, the duration of the exponential phase is varying depending on the environmental conditions and on the biological properties of the microorganisms. The exponential phase is commonly used to measure the growth rate k of the population: in fact, at early times the quadratic term in eq. (1.18) can be neglected and $\log[N(t)] \sim k\,t]$.

It should be noted that during the stationary phase the population size is constant: however, cell division does not stop to occur in this phase. Simply, the number of new cells produced by the division mechanism is balanced by the number of cells that do not divide and die, reaching an equilibrium named as **cryptic growth** [5]. For larger times, the ratio between new division and

death events starts to decrease: the **death phase** occurs. The cells die, is some cases accompanied by cells lysis and the total number of cells decrease, normally with a lower rate as the one of the exponential growth.

Biofilm in porous media

The simple model presented above is typically used to describe several scenarios, including bacterial growth within porous systems. Novel microfluidic techniques have provided to microbiology new means to study bacterial growth in porous media, allowing to directly observe the individual cells, their division inducing progress in our knowledge on biofilm development under laminar flow conditions [19]. Past studies has shown that biofilm in porous media behave in a specific way but is still understood if they act in an homogeneous way and if the structure visualized follows the logistic model presented above. As mentioned by Hassanpourfard et al. (2016) the differentiation of biofilm structures is well known under conditions of turbulent flow ($Re > 1000$) but still not well understood under conditions of laminar flow within the solid structure of a porous system.

Scheidweiler et al., (2019) have studied the growth of a natural multi-species biofilm over 220 h through time-lapse video-microscopy using stream water from Avançon river, and have concluded that bacterial population is not arranged in an homogeneous way and there is a structure differentiation in two streamers and annular base biofilm (BB). Annular base biofilm are found attached around the grains, while streamers are suspended filament of biofilm developing downstream from the grain [20]. Recent studies have concluded that the architecture of biofilm inside the porous medium is dependent on the site characteristics, and that the presence of streamers is relied to the presence of stagnant zones, so where less oxygen is present [19].

Most of recent research is focused on the understanding of streamers composition, it was identified five challenges to understand such biofilm structures and their dynamics: 1) streamer inception, 2) uncertainty of streamer evolution's colloidal hydrodynamic, 3) streamer's material properties and behavior, 4) long-term fate of streamers and as last 5) the influence of media (topography and species) on streamers formation [17]. However, it is know that the biofilm total biomass inside a porous medium can be influenced by two principal mechanism: on the one hand, cell division and microbial growth, on the other hand, the total biomass grow due filtration of suspended cell that are transported by the flow [21].

1.4 Challenges and goal of this work

Comparing the results obtained in the past through classical theory and the recent ones, different researches have concluded that the influence of the porous structure is still unknown and understanding the material behavior of bacteria and abiotic streamers may form the basis of future research. Furthermore, understanding the influence of the porous media geometry on bacterial behavior is still an open problem, which is why future research should take this into account [17].

As mentioned above, bulk studies cannot capture properly the biofilm behavior within porous media and in addition the classical system adopted since microfluidics technique has developed, where not allowing to see what was going on inside the media, but only studies the total growth because of the opaque membrane of porous media structure. Moreover, the methods used prior to microfluidics did not allow a study to be developed at multiple scales, from the macroscopic scale to the pore or bacterial scale (liquid-solid interface). From past studies it is not know if small scale bacteria organization and local environment affect macroscopic mass growth.

Knowledge of microbial transport still have many gaps due to the methods used so far. Indeed, classical theory studied cell transport by means of classical colloid filtration models without considering pore-scale processes, medium structure or microbial cell metabolism and cell division. Transport of micro-organisms is much more complex than that of colloids as they are living organisms that interact with each other and the local environment. Classical theory studied the transport and deposition of microbial cells through bench-scale or packed-column experiments, where the concentration of microbes in a solution was monitored as a function of time [13, 14].

Several critical reviews for traditional models for microbial transport and growth have been proposed (e.g. of Tufenkji (2006) and Bradford et al. (2014)) : while microbial transport in water is controlled by advection, diffusion and mechanical dispersion, to couple these processes with cells division, attachment and filtration is still an open problem. Here, by means of microfluidics experiments and time-lapse video-microscopy, I investigate the growth of a bacterial isolate initially homogeneously present in all pores of a homogeneous porous system, systematically studying their spatial distribution that varies in time and space due to nutrients and oxygen availability under laminar and stationary flow conditions.

Chapter 2

Methods

2.1 Experimental set-up and overall strategy

This project aims at studying the temporal dynamics and spatial distribution of bacterial biomass exposed to constant and laminar flow trough porous media. I consider two different transport conditions: the experiments will be carried out in a confined and homogeneous porous system represented by a transparent microfluidics allowing to detect location of bacterial cells as they grow. The following method is applied in order analyze the overall biomass growth under imposed flow of nutrient and oxygen water-solution, simultaneously, at macroscopic and microscopic scale.

The objective is to temporally and spatially quantify bacterial growth in a confined porous structure with i) a constant injection of a sterile solution of nutrients and ii) a constant injection of a bacterial suspension. Each experiment last for about 24 hours and are of three types, all three replicated three times. The first type of experiment was carried out to test the growth conditions of the bacteria and to check that without flow the bacteria grew homogeneously. The other two experiments were carried out with different strategies. First, the porous medium was saturated with a bacterial suspension, then, a sterile nutrients solution was injected for 24 hours. Second, the porous medium was saturated only with the sterile nutrient solution, then, a bacterial suspension with the same nutrients concentration was injected.

To extend the results beyond classical bulk studies, that cannot access information on spatial organization of bacteria, biomass is studied through transparent replicas of porous media with microfluidic technique. This innovative method makes possible to carry out a multi-scale analysis and to analyze what is happening inside the porous system.

2.2 Microbial strains and protocols

A non-flagellated mutant of *P. putida* bacteria, KT2440 ΔfliM, tagged with green fluorescent protein (GFP) embedded into their DNA together with Gentamicin antibiotic resistance. These bacteria are non-pathogenic and are very common in soil systems [22]. Colonies were initially grown from frozen stock, consisting of 50% glycerol and 50% water-suspension of bacteria, stocked at -80°C. Colonies were grown on a autoclaved Petri dishes consisting of Luria-Bertani broth (LB, Lennox solubility 20 g/L H_2O, *Sigma-Aldrich*), Agar (Agar 15 g/L *Difco*) and the antibiotic Gentamicin Sulfate (AG, 10 mg/L to avoid microbial contamination); they were incubated at 30°C for 24 hours and then stocked in the refrigerator at 4°C.

Bacterial liquid cultures were prepared with a base of 4 mL of LB nutrients solution and 4 μL AG antibiotic, in which were added a colony of *P. putida*. This initial solution was shacked overnight at 180 RPM and kept at 30°C. Then, the solution was diluted: 20 µL of the overnight solution were added to 4 mL of LB05 and 4 µL AG and then directly used for the flow experiments.

Overnight culture was grown inside pure LB (following produced manufacturer instructions) and then diluted inside in a LB and milli-Q water mixture (50% and 50%, respectively LB05): the pure LB is has concentration of 20 g/L of in milliQ-water, LB05 has a concentration of 10 g/L. Manufacturer instructions form *Sigma-Aldrich* are to suspend 20 g of LB in 1 L of distilled water, autoclave for 15 min at 121°C.

The first injection strategy (strategy 1) consists of infecting and saturating the chip with the prepared bacterial suspension: once the entire porous medium has been saturated, I start injecting a sterile solution of nutrients and antibiotic (LB05 + AG), in this way the biomass present and observed inside the chip is due to cell division and not to the injection of new cells. The second injection strategy consists in saturating he chip with sterile nutrients and antibiotic, then, the prepared bacterial suspension was constantly injected at the same flow rate Q. With this second strategy, the biomass accumulating within the system is due to cell division but also to the constant injection of new cells.

2.3 Microfluidic devices to mimic a porous environment

To reproduce biofilm formation in a ad-hoc designed porous environment, a polymethylsiloxane (PDMS) microfluidic chips were fabricated: PDMS is made of the *Sylgard 184* Elastomer Kit. The

liquid PDMS was mixed with its curing agent (from the same kit) in proportion 10:1 by weight to obtain a three parallel channels with identical porous matrix composed of vertical cylindrical pillars, acting as grains. The master on which the PDMS chip has been fabricated was developed using standard lithography.

In each channel the porous matrix occupy 50 mm (L) by 7 mm (W) and it is thick 0.05 mm, for a transversal area (A=wh) of 0.35 mm^2 and a pore volume (PV) of 8.75 min. The porosity, ϕ, of the system is about 50% and the grains are disposed along the channel at the edges of a regular lattice with a total of 19 by 76 grains. The three channels have independent inlets and outlets and can be simultaneously controlled. The fluid flow inside the channels is controlled with a syringe pump (Standard Infuse/Withdraw Harvard Apparatus *PHD ULTRA*) which allows to impose a constant flow. The used syringes, one per channel, are single-use made of plastic (HSW HENKE-JECT 5 ml, Luer-Lock), which increases the responsiveness of the systems to flow rate changes [20]. To connect each syringe to the channel I have used a Tygon tube (COLE-PARMER Tygon Tubing, inner diameter of 0.5 mm, outer diameter 1 mm).

The experiments were carried out using the two strategies described above, in order to study the growth rate and biofilm local organization between those paradigmatic cases. In the first strategy (strategy 1), the chip was infected with bacteria and a sterile nutrients solution was injected for the entire duration of the experiment with a constant flow rate Q. In the second case (strategy 2), the chip was saturated with sterile nutrients solution, then, the prepared microbial suspension was constantly injected at the same flow rate Q for the duration of the experiment. For both strategies the imposed flow was $Q = 1$ µL/min. In addition, the experiments were carried out at a constant temperature of 30°C, exploiting the temperature controller present around the microscope stage (OKOLAB microscope enclosure).

2.4 Optical time-lapse video-microscopy

To capture a series of time lapse large-images I used an automated and inverted microscope (Nikon ECLIPSE T*i*) equipped with a sCOMS camera (Hamamatsu ORCA flash 4.0) and 4X or 10X objective magnification, depending on the type of acquisition, as specified below. The images were acquired using fluorescent and phase contrast microscopy, in order to analyze i) the intensity of the emitted fluorescence as proxy for the volume of biofilm. The GFP proteins produced by the used isolate strain, have absorption peaks at 395 nm and emission about 475 nm. The camera has pixels of size

of 6.5 by 6.5 μm organized as an array of 2048 by 2408 pixels. The effective area of an image is about 13.3 by 13.3 mm.

I have acquired a series of 33 large-images during 24 hours: during the first 3 hours I collected a picture every 20 minutes, then, every hour. Each large-image is a composition of 3 by 8 pictures that are tiled together automatically by the software controlling our automated scope (Nikon Elements) that moves and collects all the pictures to cover the whole porous area. This timing was chosen in order to have a frequent acquisition during early times when it is expected the exponential growth phase discussed in the introduction chapter. Based on preliminary tests I performed with these bacteria grown with the described protocol, I expected that within the confined space of a microfluidics the exponential phase can last up to three hours. Once the steady state was reached, the images were acquired every hour so that I could study the later growth.

2.5 Flow system

The hydraulic proprieties were chosen to get laminar flow conditions, defined by the Reynolds number ($Re \ll 1$). The Reynolds number is a parameters which defines the flow regime: low Re means laminar flow and high Re means chaotic or turbulent one [23]. It is defined as $Re = \lambda q/\nu$, where ν is the fluid kinematic viscosity [mm^2/s], q the average fluid velocity of the [mm/s] and λ is the characteristic space over which the fluid velocity varies, here the average pore size [mm]. For a flow rate $Q = 1$ mm^3/min, the characteristic time needed to flush a whole pore volume is $t_{PV} = V/Q$ and the average fluid velocity $q = 2.86$ mm/min (q = Q/A); since the kinematic viscosity of water is $\nu = 1$ mm^2/s, the Reynolds number is $Re = 0.006$ mm/s, meaning that it is a laminar flow, for $\lambda = 130\,\mu$ m.

2.6 Image acquisition and analysis

Using optical microscopy, 3 replicas of images were acquired for both strategies, with a total duration of 1440 minutes. The acquired large-images were processed using a Matlab script. In order to carry out the analysis of the results, the first image of each data set was used to extract a binary matrix, called the mask, composed zeros and ones representing grains and pores, respectively. This matrix allows us to remove all grains from each large-image ad process only the data within the pores. The following image shows the binarization process of the first image, converted into the mask matrix. The first step is to calculate the threshold intensity which characterizes if a pixel rep-

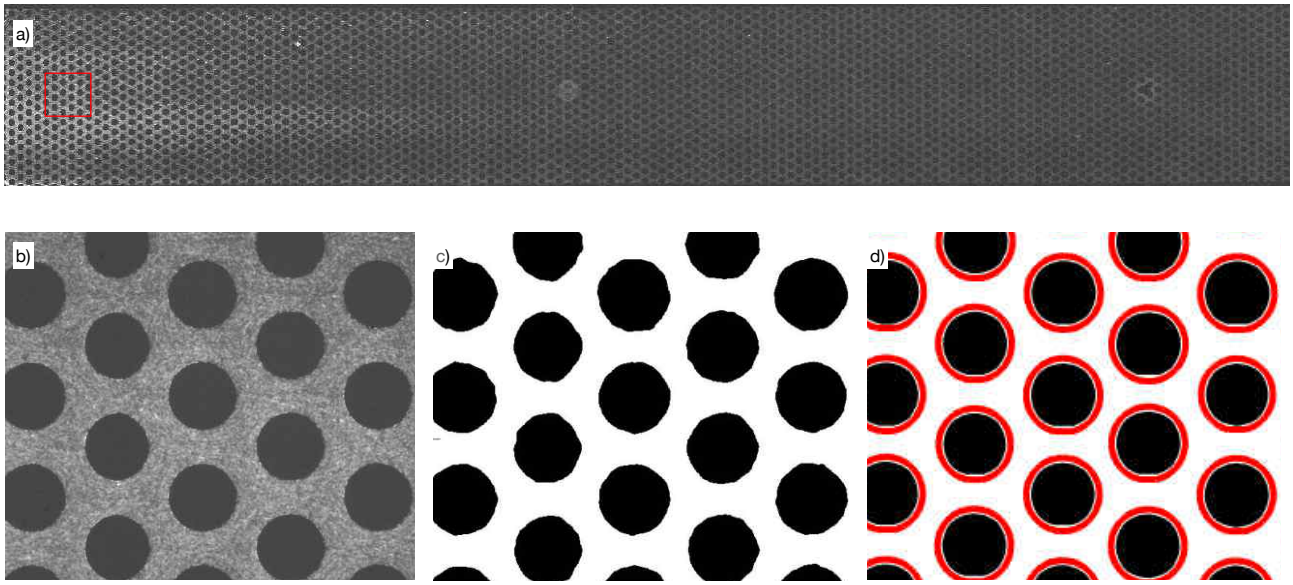

Figure 2.1: *a*. Original image acquired at the first time step during the cultivation of bacteria. *b*. Section of the original image. *c*. Section of the binary image (black = 0, white = 1). *d*. Circumference of the grain in red extracted with the immage procession (*red*)

resents a grain or a pore using the original image (figures 2.1.a and .b), then, once the binary image is extracted (figure 2.1.c), with the function *regionprops* in MATLAB, the centers and radius of each grains are detected and saved as matrix (figure 2.1.d) for future image processing. The same procedure was used to process the entire data sets. Images acquired in fluorescence and having a gray scale brightness intensity were converted to binary images and everything considered biomass was given a value of 1, the rest a value of 0. In order to binarize the images, a threshold was calculated, which defined for each image pixel whether it was covered by biomass or not. A local adapted threshold was calculated for each pixel based on the mean intensity in the close neighborhood of each pixel.

In order to carry out a complete analysis, it was necessary to develop a code that could recognize the different biofilm architectures expected during the flow experiments. Once the binarization of the first image and the identification of the grains and their radii and centers had been carried out, it was possible to proceed with more complex analyses. As with binarization, an adaptive threshold was calculated on the first acquired image in time, with a square area of 1501 pixels.

Biofilm architecture differentiation. To distinguish the biofilm into its constitutive architectures, I, first, identify the base biofilm (BB) around each grains. I wrote a Matlab script to analyze the biomass at the pore scale, grain by grain. For each grain, I considered a annular ring of inner radius

equal to the one of the grain r_g, while its outer one R_n is defined grain by grain based on the biofilm aroun it. The two radii, inner and outer, thus represent the radii of the inner and out circumferences of a ring defined as the larger one whose area is at least 40% covered by biomass, as described in [19]. The annular ring thickness R_n depends on the amount of base biofilm detected around each grain: in fact, its outer radius R_2 is defined with a loop over the index n so that:

$$R_n = r_g + n\,\delta R \tag{2.1}$$

where $\delta R = 1$ pixel is a radius increment that I used to compute the biomass present within the annular ring from r_g and $r_g + n\,\delta R$. The outer annular ring radius R_2 increases within a loop over $n = 1, 2, 3\ldots$ while the biomass surface within that annular ring exceeds 40% of the ring area, then it stops defining the outer BB radius. As soon as the detected biomass surface coverage is below 40% of the annular ring considered, the calculation stops and the BB external radius is R_n. If the biomass surface stays below 40% of the annular ring surface, the loop continues up to a maximum radius of $R_{max} = 60$ pixels, and if even within this ring not enough biomass is found, then, the ring is considered empty (without BB) and the calculation continue with the next grain.

Once the presence of BB has been calculated around each grain, two matrices are created, both binary (values equal 0 or 1): 1) the first one records as value 1 all pixels considered BB, and zero for all the rest, and 2) a matrix that at each pixel has value 1 where biomass has been recognized but it was not considered BB by our algorithm and zero for the rest.

This first calculation allows the recognition of all the grains surrounded by BB, and the amount of biomass contained in it, in fact the binary matrix is multiplied by the value of the fluorescence intensity recorded in each pixel of the original images, in this way where there is biomass the pixel value is multiplied by a value of 1, and where there is no biomass by a value of 0. The calculations performed so far have made it possible to extract the biomass architecture dynamics and its spatial occupancy in terms of BB, no BB and total.

Macroscopic longitudinal organization of the biofilm and its architectures. After having done this pore-scale analysis, I computed the deposition profile (eq. 2.2) from each time, for each biofilm architecture (BB and no BB) and total biomass. The integral of the binary image was calculated and divided into 200 intervals.

$$DP = \int_{i}^{i+200} (\sum_{i}^{i+1} BB) \tag{2.2}$$

For each interval along the x-axis of the matrix (longitudinal, main flow direction along the processed images) it is calculated the biomass integral: total, BB and no BB (meaning subtracting the BB biomass from the total biomass). The transverse integral defined by eq. (2.2) of the biomass is divided by the DP of the mask, in order to take into account the detailed pore size. The deposition profile is useful to understand in which portion of the porous system the biomass is organized as a function of distance from the inlet.

The limit of BB-dominated zone. Using the function *bwboundaries* Matlab function, it was possible to plot the outer limit of an area near the medium inlet that was clearly dominated by the presence of BB architecture. Outside this area, the biofilm was mostly organized not as BB, but differently, as streamers or deposited on the chip ground also forming ripples, as sand dunes. We observed this behavior in all replicas and all injection strategies, as discussed below.

The outer limit of this area seems to have a parabolic shape, as shown in figure 2.2.a. To systematically define the limit of such area, I used the matrix defining the BB around the grains: removing the isolated clusters it is possible to convert it into a binary matrix with a value of 1 inside the BB-dominated area and 0 outside (figure 2.2.b). The Matlab function *bwboundaries* is, then, used to find all x and y coordinates of the outer perimeter (red line in figure 2.2.b, green in figure 2.2.c).

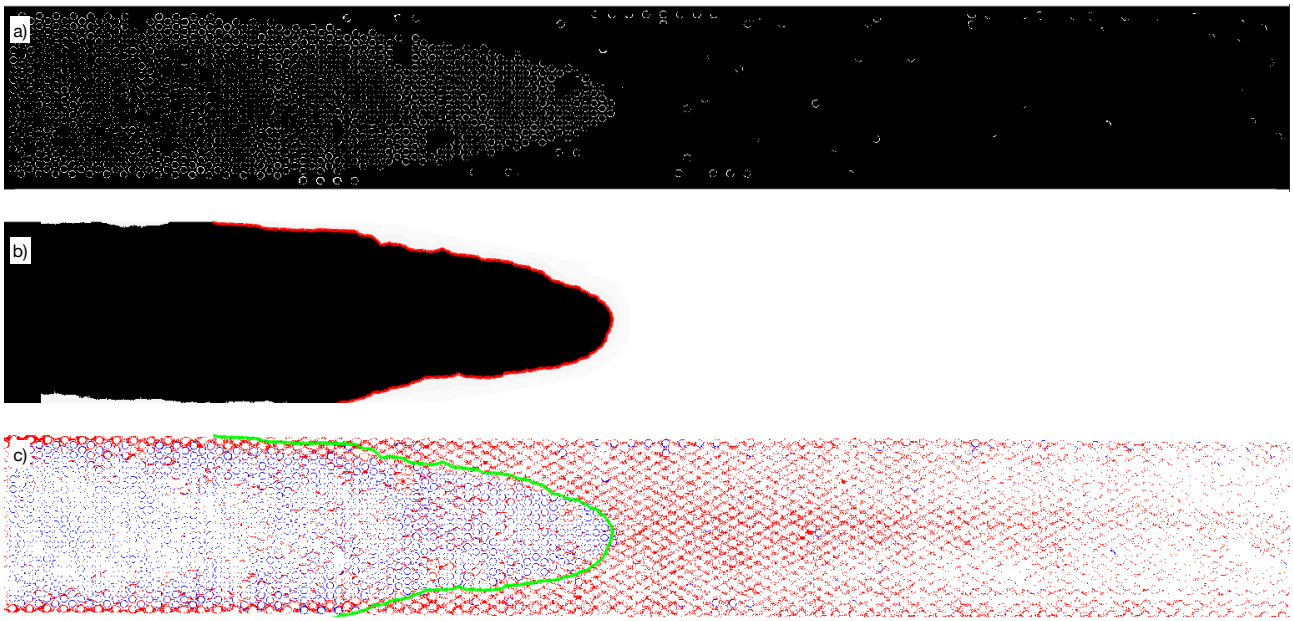

Figure 2.2: *a*. Base biofilm matrix extracted from the image acquired during the experiments. *b*. Extraction of the Base Biofilm dominated area, with a parabolic-like shape from the base biofilm matrix. *c*. Extraction of the coordinates of the point on the external profile of the BB dominated area, overlaid on the base biofilm and no BB matrix.

Chapter 3

Results

This chapter presents the experimental results obtained with the method and procedure discussed in the previous chapter. In order to understand what processes have control the biofilm architectural dynamics and spatial distribution within porous media, the acquired data processing is divided into a qualitative and a quantitative analysis. The qualitative description our our results makes it possible to identify the main processes controlling the diversification of architectural structures within the porous media at the microscopic scale (pore scale) but also at the landscape scale (the one of the entire porous system). Then, with the qualitatively identified structures and processes, detailed measurement were developed to sustain the quantitative description.

On the one hand, the qualitative description consists of observing the large-images series acquired (three replicas) during the experiments and drawing consistent explanation in order to understand what phenomena controls the observations and should be quantified. On the other hand, quantitative description is based on the phenomena visualized qualitatively, to derive systematically information (average deposition profile, spatial and temporal biomass distribution, ...). The description of our results, reported below, is done separately for the two injection strategies, as different biofilm structures emerge. For the seek of presenting the results, only one of the three replicas has been selected to be shown here for each injection strategy, but the results were consistent over the triplicate. Once the diagnostic quantities to be measured have been identified, our quantitative results will be shown in terms of their mean value over the replicas.

As discussed below, the macroscopic diagnostic quantities selected to track the biomass are the growth curve, the biomass profile as function of distance from inlet and the porous area dominated by the BB architecture. At the pore scale, the location where biofilm architectures develop over time (in terms of base biofilm and total biomass) are computed and shown. In both injection strategies

and scale of observation (micro and macro), the results obtained are shown in similar organization, initially presenting the qualitative analysis and, then, the quantitative one.

3.1 Qualitative description of microbial mass growth

3.1.1 Bacterial growth without flow

The images acquired during the experiment with no flow show that with LB05 medium, cells division takes place within the confined space of the microfluidics: over time the individual cells become larger cluster composed by several cells. Indeed, figure 3.1 shows that, with a 20 minute difference between each acquisition, the number of individual cells increases over time. After about 100 min the biomass doesn't seem to grow anymore.

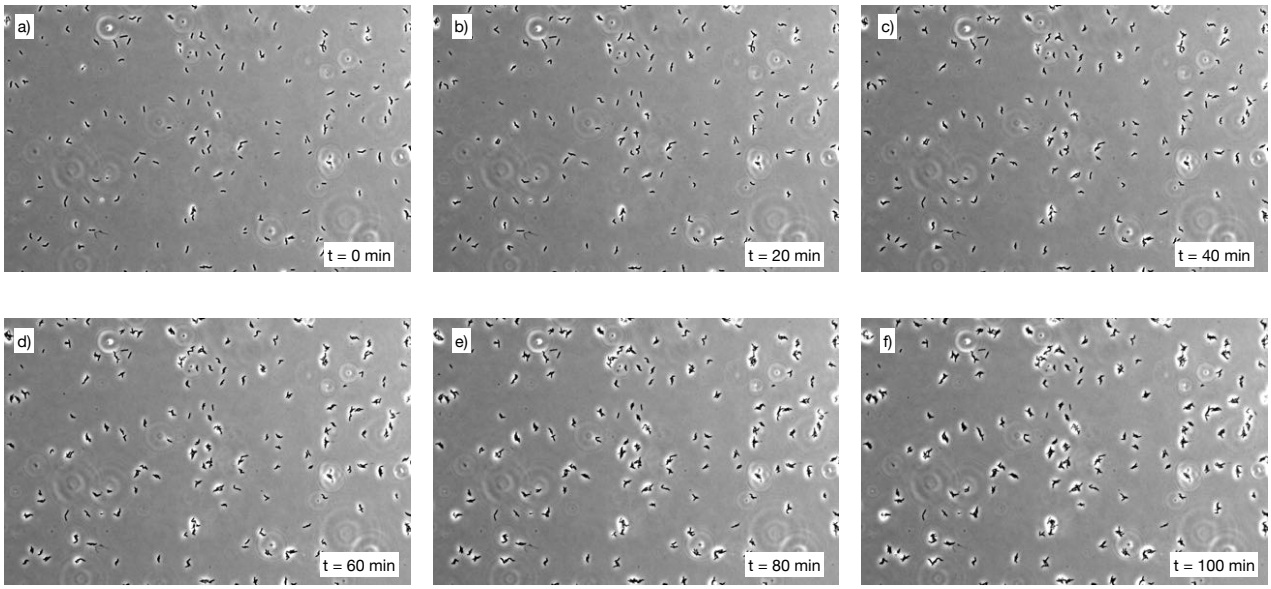

Figure 3.1: Bacteria culture growing in a non porous channel without flow with 50% nutrients (LB) concentration. *a*. At time 0, *b*. After 20 min, *c*. 40 min, *d*. 60 min, *e*. 80 min and f. 100 min.

3.1.2 Injection strategy 1

Thanks to the images acquired over time at specific intervals, five crucial acquisitions were identified, which shown important phenomena and structural diversification. As the porous system has been infected with the prepared bacterial suspension and the nutrient-antibiotic solution was continuously injected eluting 1 pore volume, all the susepnded bacteria were displaced away from

the outlet and only those cells that attached to a surface (a grain, the chip ground or its ceiling) are still in the system and optically visible. Figure 3.2) shows that after eluting 1 pore volume the concentration of bacteria throughout the whole medium seems homogeneous, both longitudinally and transversely. In other words, all pores have the same amount of bacteria attached to their surfaces.

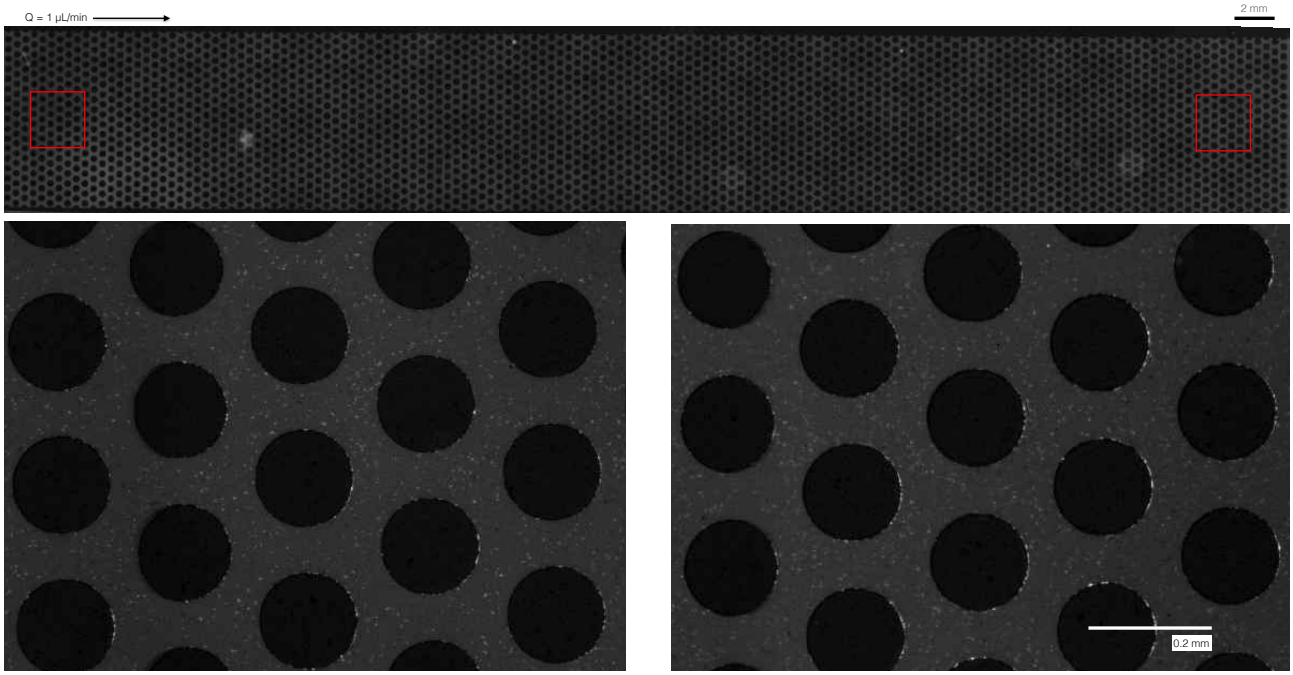

Figure 3.2: Strategy 1, image acquired after 1 pore volume in fluorescence and subsection of the images near the inlet (left) and outlet (right).

Later, after injecting 34 porous volumes (corresponding to 5 hours) of the nutrient-antibiotic solution, figure 3.3) shows that the fluorescence signal coming from the area near inlet is strong while it decays monotonically while moving towards the outlet area. Also, the pore scale bacterial organization seems to be homogeneous locally, but it varies when moving from the inlet towards outlet. This fluorescent signal variability along the longitudinal direction (i.e. from inlet towards the outlet), can be linked to a clearly different biofilm architecture in each pore. Near the inlet biofilm seems to be growing on the chip ground and grains surfaces and Base Biofilm can be clearly identified, while near the outlet less growth takes place and smaller individual colonies can be detected without covering large surfaces or significant fractions of the grains surface.

Even later, when 54 pore volumes have been eluted (corresponding to 7.9 hours), it is possible to clearly distinguish the area dominated by growth of BB and the rest of the system not dominated by such biofilm architecture. A parabolic-like area pointing towards outlet can be well recognized (as

shown in figure 3.4). This BB-dominated area has a macroscopic structural difference with respect to its outer region. In fact, within this area in addition to the appearance of the BB, we observe the formation of elongated biofilm structures, individual streamers, homogeneously downstream each grain while each BB have increased the outer radius becoming optically well defined. Outside the BB-dominated region, the biofilm has coated the chip ground with a homogeneous architecture that repeats longitudinally and transversely. We also observe that these biofilm architecture shows the formation of ripples-like structure (as in sand dunes), probably induced by the constant fluid flow.

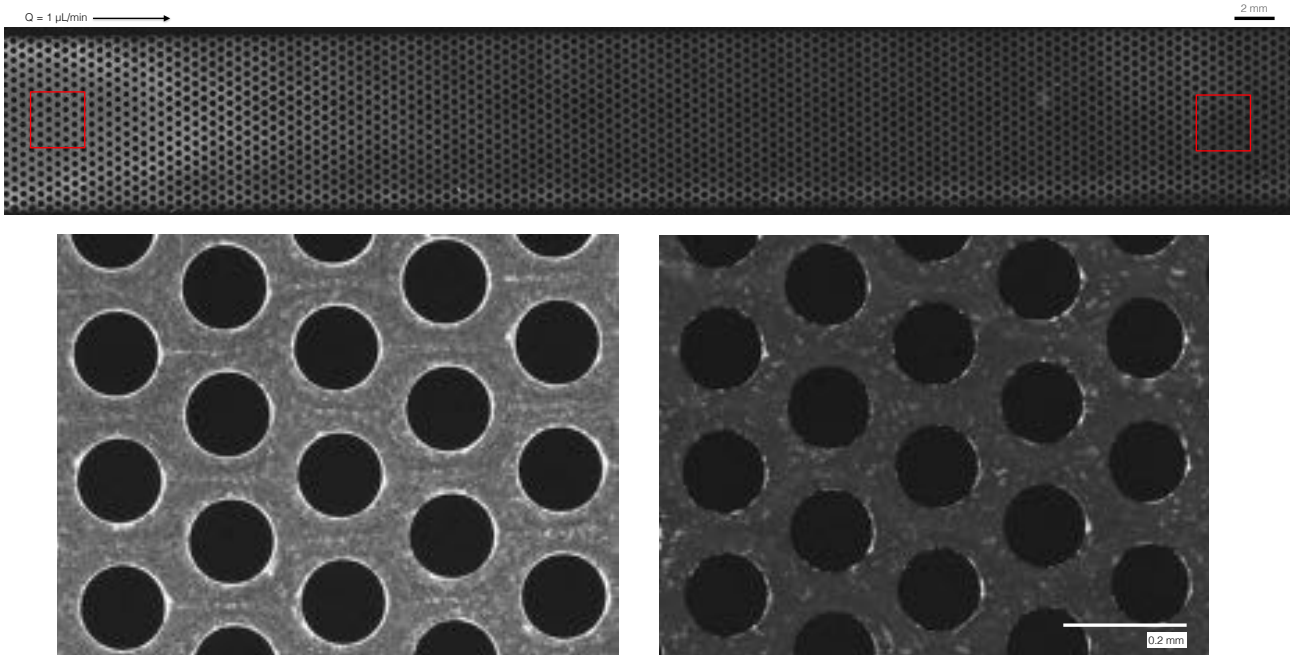

Figure 3.3: Strategy 1, image acquired after 34 pore volume in fluorescence.

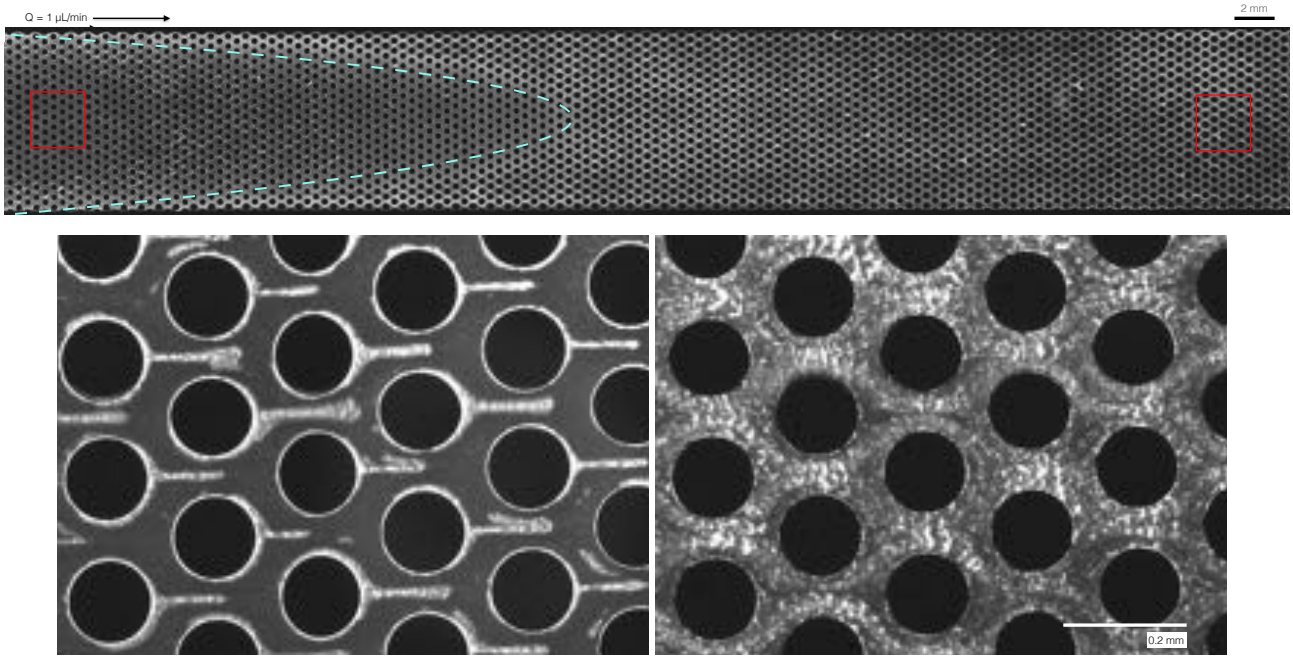

Figure 3.4: Strategy 1, image acquired after 54 pore volume in fluorescence.

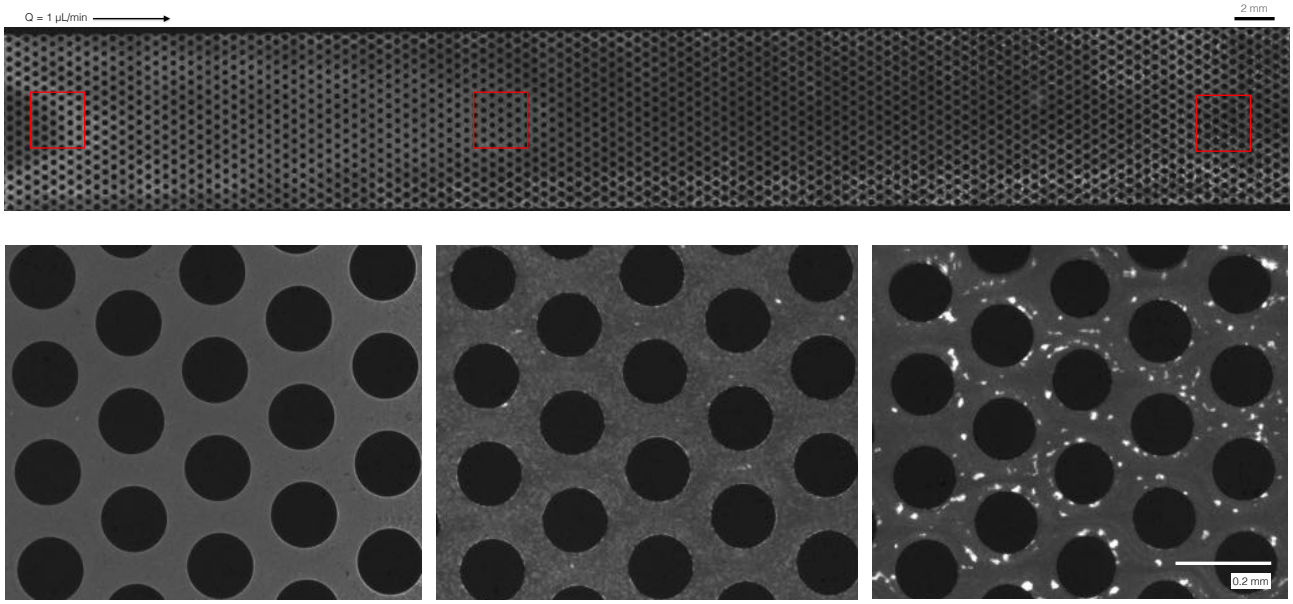

Figure 3.6: Strategy 1, image acquired after 164 pore volume in fluorescence.

After constant injection for 130 pore volumes (corresponding to 19 hours) the biofilm structure differentiates into three different architectures (as shown in figure 3.5). Near the inlet and within

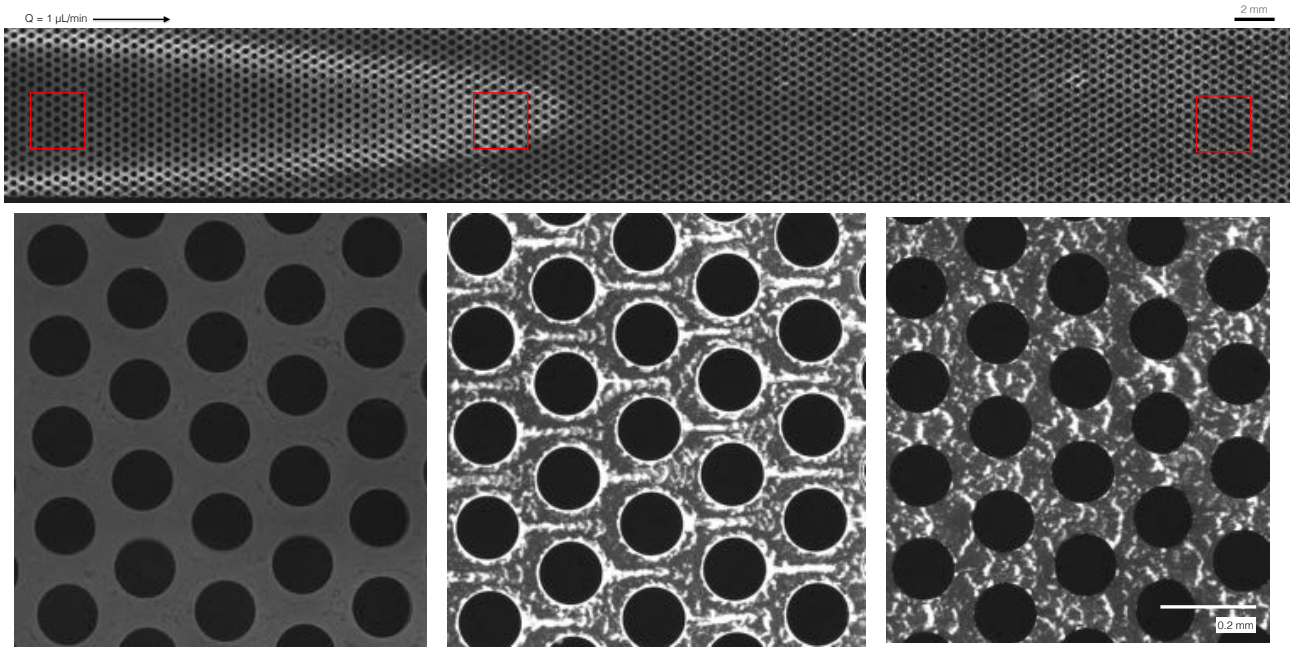

Figure 3.5: Strategy 1, image acquired after 130 pore volume in fluorescence.

the region previously BB-dominated, the fluorescent signal of the cells becomes homogeneous and loses intensity, a well-defined biofilm architecture cannot be detected any more. At the front of the dish, over a width of 3 to 6 grains, there are still base biofilm and streamers downstream at the grain, but much less defined, they seem to begin to degrade and ripples begin to be identified. Outside the BB dominated area to the outlet the structure is the same over the whole area and ripples are identified between the grains. In the last image acquired (figure 3.6), after 164 pore volumes, the fluorescence intensity decreases along the entire porous media and all structures observed up to that point have degraded, one can still see a diversification of structures longitudinally, but much less clearly than before.

3.1.3 Injection strategy 2

For the second strategy, as for the first, five fundamental acquisition for diversification were identified. After injecting the prepared bacterial suspension into the nutrient-antibiotic saturated medium for a time equivalent to eluting 17 pore volumes (corresponding to 2.5 hours), it is clearly visible a difference in the detected fluorescent signal emitted by bacteria between inlet and outlet. The cells signal shows a higher bacterial abundance near the inlet, the signal intensity decreases monotonically while moving towards the outlet, as shown in figure 3.7.

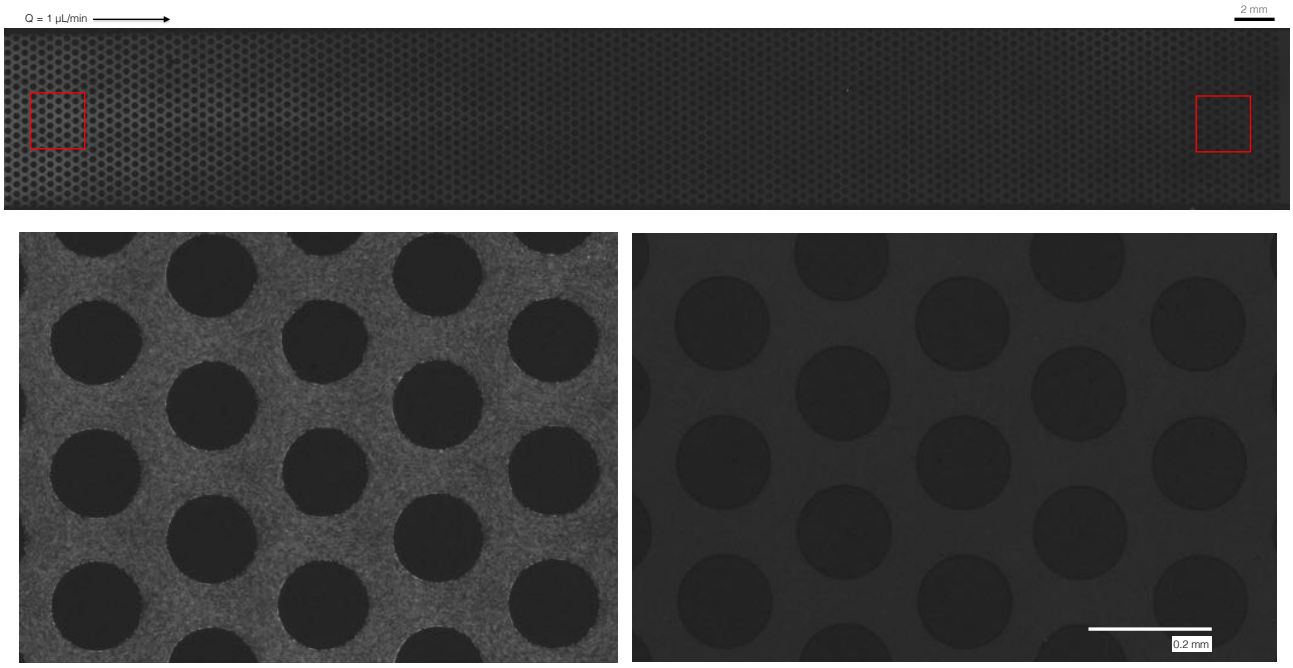

Figure 3.7: Strategy 2, image acquired after 17 pore volume in fluorescence.

After eluting 24 pore volumes (corresponding to 3.5 hours), it appears a biofilm organization change near the inlet: as shown in figure 3.8, the fluorescent signal intensity increases near the inlet, while the one near the outlet stay about the previous values. Cells are starting to fill all the pore spaces creating a homogeneous biomass distribution near the inlet, where it is visible a thin ring forming upstream of each grain. Near the outlet we detect very little biomass.

After 41 pore volumes are eluted (corresponding to 6 hours), figure 3.9 shows the emergence of a zone dominated by BB near the inlet, as observed for the injection strategy 1, whose downstream boundary have a parabolic-like shape. These BB is also characterized by having a wavy contour with, downstream from the grain, a thinner layer of biofilm, a gap, as observed in [19]. As shown in figure 3.9, beside the BB around each grain, biomass is also visible within the pore space and in focus, thus on the chip ground, organized in very thin, i.e. about $5 - 8\,\mu$m, filament like structures, now called ripples, that seem to connect BB among grains. These two structures, ripples and BB, are homogeneously present inside the BB-dominated area. While we still detect little biomass, at the outlet the number of cells start to slowly increase: outside the BB-dominated area the biomass is organized in scattered colonies, apparently not connected among each other.

After 61 pore volumes were eluted (corresponding to 9 hours), the biofilm architecture within the

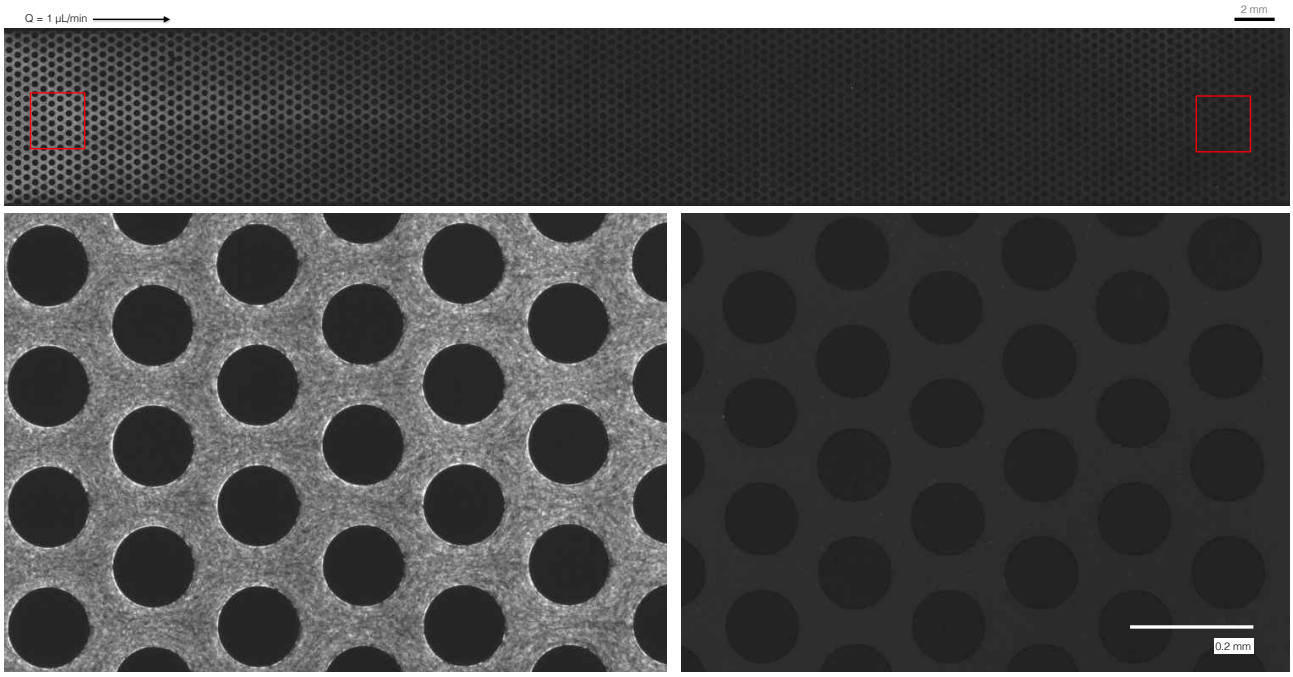

Figure 3.8: Strategy 2, image acquired after 24 pore volume in fluorescence.

porous system appear to be divided into three structures, as shown in figure 3.10. It is observed that within the BB-dominated area, the previously observed ripples have degraded and streamers-like biofilm, composed of two elongated structures attach to a grain and protruding the pore space downstream, emerge homogeneously. At the same time, the BB appear to have a finer radius than before. Just outside the outer boundaries of the BB-dominated area we observe two other structures: ripples and a carpet of colonies that, due to their growing size, merged. The ripples emit a more intense fluorescent signal than those observed earlier, around 41 pore volumes, within the BB-dominated area. Near the outlet the biofilm architecture seem to be not connected to the grain structure and it is homogeneous among the pores: it looks like that the individual colonies grew and merged into a carpet emitting a slightly higher fluorescent signal than the one near the outlet for earlier times.

After 164 pore volumes were eluted (corresponding to 24 hours), the fluorescent signal decays and becomes homogeneous throughout the chip. No specific biofilm architecture is observed within the porous system.

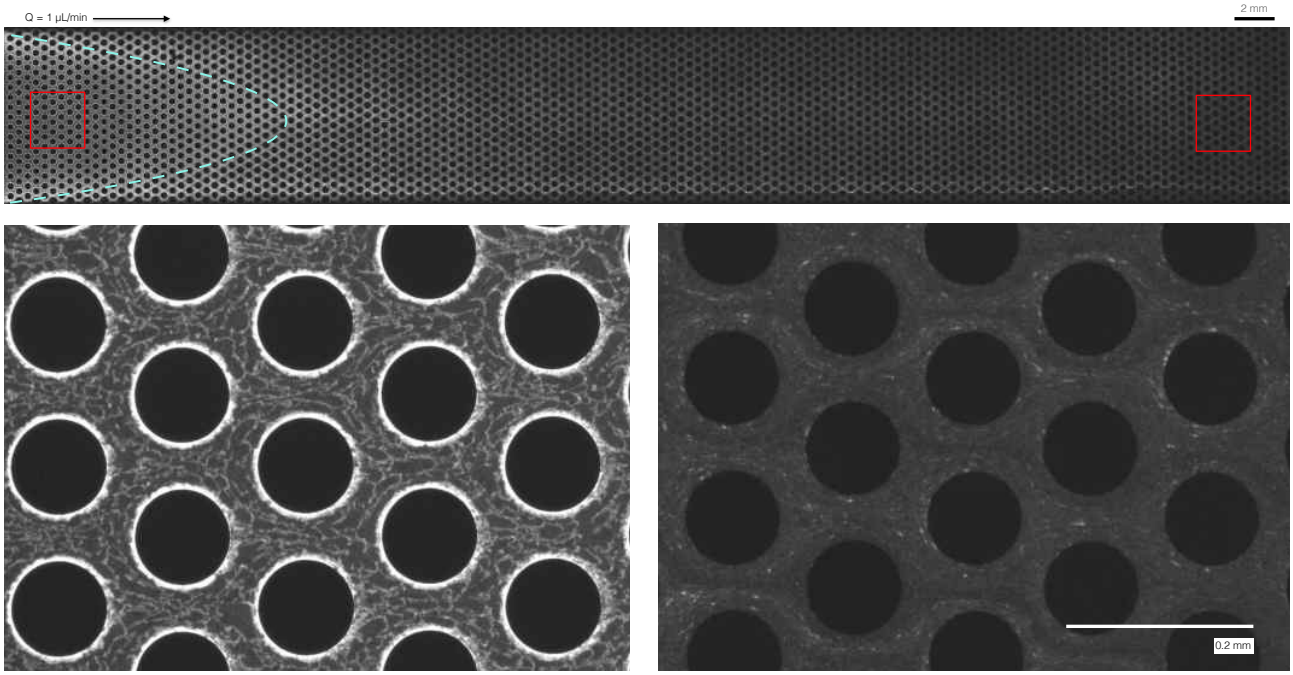

Figure 3.9: Strategy 2, image acquired after 41 pore volume in fluorescence.

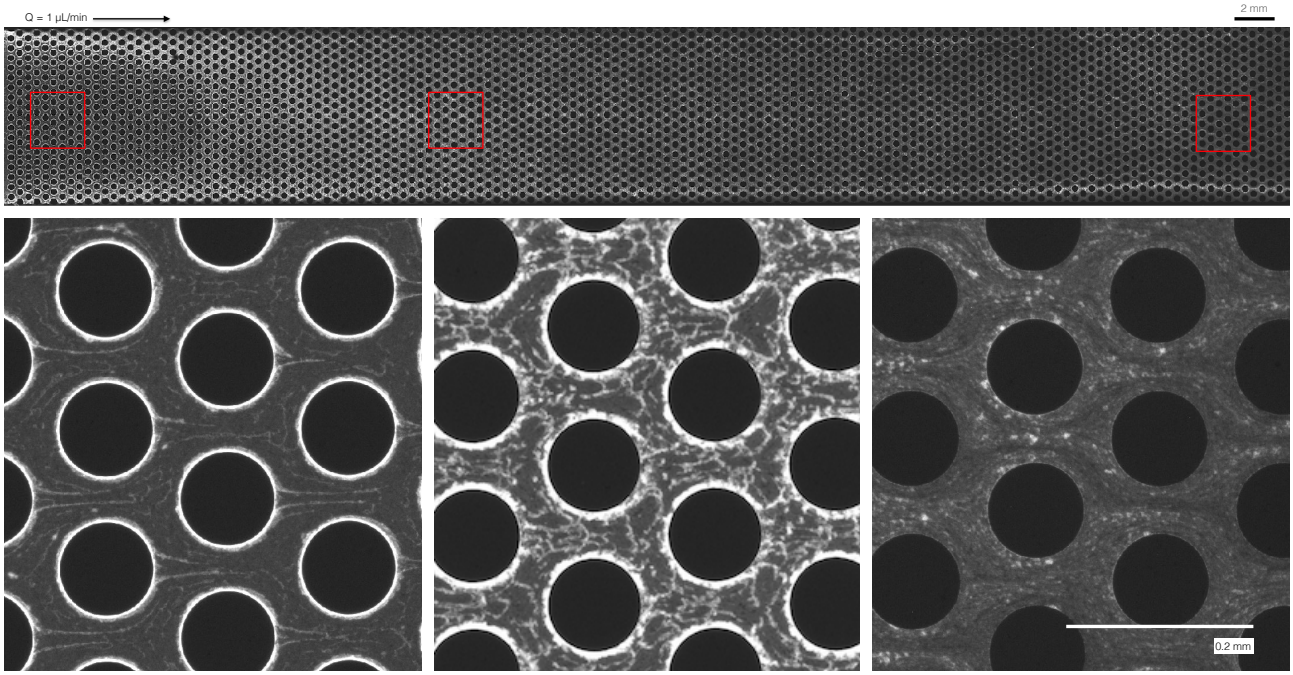

Figure 3.10: Strategy 2, image acquired after 61 pore volume in fluorescence.

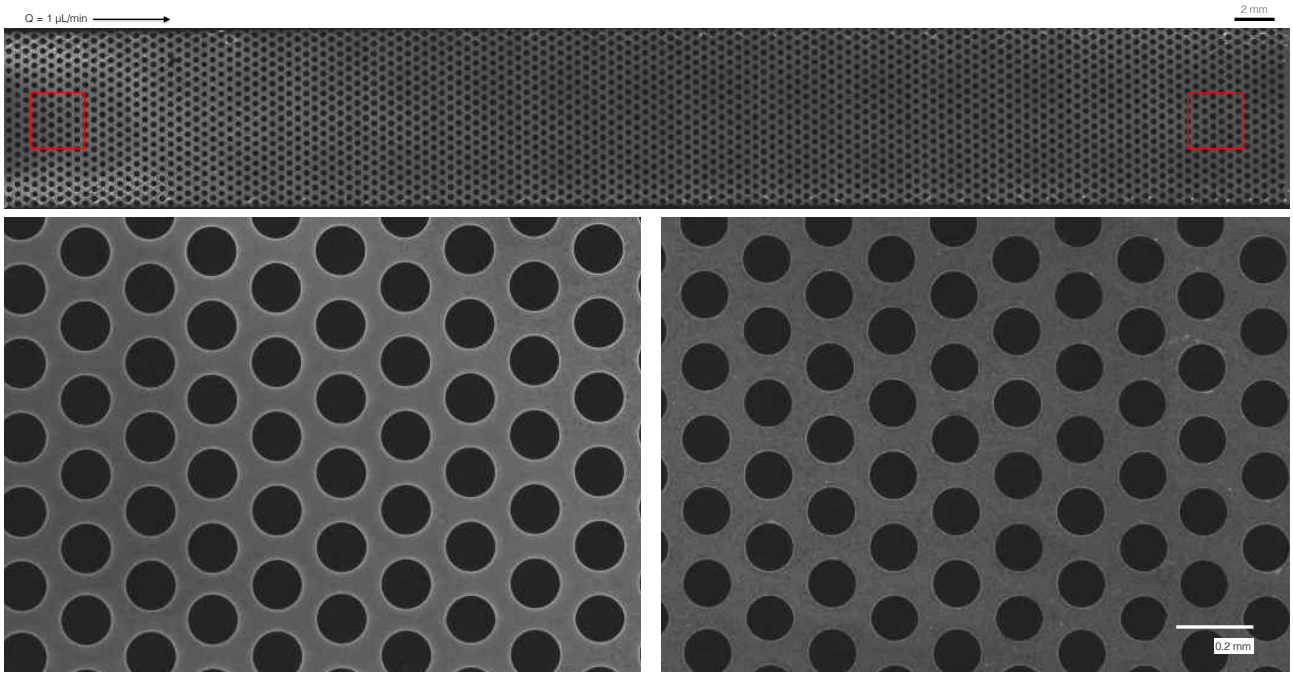

Figure 3.11: Strategy 2, image acquired after 164 pore volume in fluorescence.

3.1.4 Comparing the qualitative observations

The two injection strategies results in some similarities and some difference, as compared in table 3.1 and 3.2. In both scenarios we observed the emergence of a BB-dominating area near the chip inlet with a parabolic-like shape pointing towards the outlet. The biofilm structure observed within this BB-dominated area is different from the one that develops outside.

On the one hand, the injection strategy 1 shows a constant change in the fluorescent signal intensity of emitted by the cells: the observed structures are, going from the inlet towards the outlet, BB, single streamers-like structures developing downstream each grain and ripples. On the other hand, with the injection strategy 2 there is an initial heterogeneity in biomass distribution (more cells are observed near the inlet) and with time we observe the emergence of a structural differentiation, especially after the appearance of the BB-dominated area. Inside this area, we observe ripples (which we did not injecting a sterile nutrient solution) and later a double streamer-like filament downstream each grain (which is also surrounded by BB). Outside the BB-dominated area, the biomass distribution remains homogeneous, throughout the experiment, as individual colonies that eventually merge into a carpet of cells, without developing any ripple-like structure.

Table 3.1: Observed structures with strategy 1

Time	Location	Structure
1-30 PV	Entire porous surface	Initial homogeneous concentration
54 PV	First half of the system	BB dominated area
54-130 PV	Ouside the BB dominated area	Ripples
54-100 PV	Inside the BB dominated area	Single streamer downstream the grains
54-100 PV	Inside the BB dominated area	Base Biofilm
130 PV	Along the BB dominated area	Base Biofilm
130 PV	Along the BB dominated area	Single streamer downstream the grains

3.2 Quantitative results: integrated image processing

Based on the qualitative analysis presented in above, I defined the processes I suppose control the biofilm architecture emergence within the porous system that I now quantify. To make a quantitative description at the pore (microscopic) and landscape (macroscopic) scale, the following I measured the quantity defined below, for both injection strategies.

3.2.1 Strategy 1

For each replica, I measured via image processing, as detailed in the previous chapter i) the deposition profile that it is plotted as a function of distance from the inlet, ii) the average biomass distribution (among the 3 replicates) that it is also plotted as function of distance from the inlet. Since the image processing I developed allowed me to distinguish the biomass structure between BB and the rest, both previous quantities were calculated for BB and the rest, separately, so that the sum of these two is equivalent to the total biomass.

Table 3.2: Observed structures with strategy 2

Time	Location	Structure
17 PV	Entire porous surface	Initial heterogeneous concentration
24 PV	First half of the system	Homogeneous biomass distribution
24 PV	Secon half of the system	Zero biomass distribution
41 PV	Inside the BB dominated area	Base Biofilm
61 PV	Along the BB dominated area perimeter	Base Biofilm
61 PV	Inside the BB dominated area	Double streamer downstream the grains
165 PV	Entire porous surface	Homogeneous biomass distribution

Figure 3.12 shows the average deposition profile for the BB coverage as function of the distance from the inlet in mm, everything not considered BB is plotted separately. The average deposition profile is plotted for the acquired time loop number 1, 5, 9, 13, 17, 21, 25, 29, 33, going form cyan to pink. Figure 3.12.a shows the deposition profile for the BB biomass coverage, figure 3.12.b shows the biomass that is not BB and figure 3.12.c the deposition profile for total biomass.

The longitudinal distribution of BB, averaged over the three replica shown in 3.12, from the inlet it increases to reach a peak around 15-20 mm, then it decreases as we move towards the outlet. Only at late times, after xxx pore volumes have been eluted, some BB emerge near the outlet. The biomass that is not recognized as BB dominates onlt for distances larger than 15-20 mm, monotonically increasing towards the outlet.

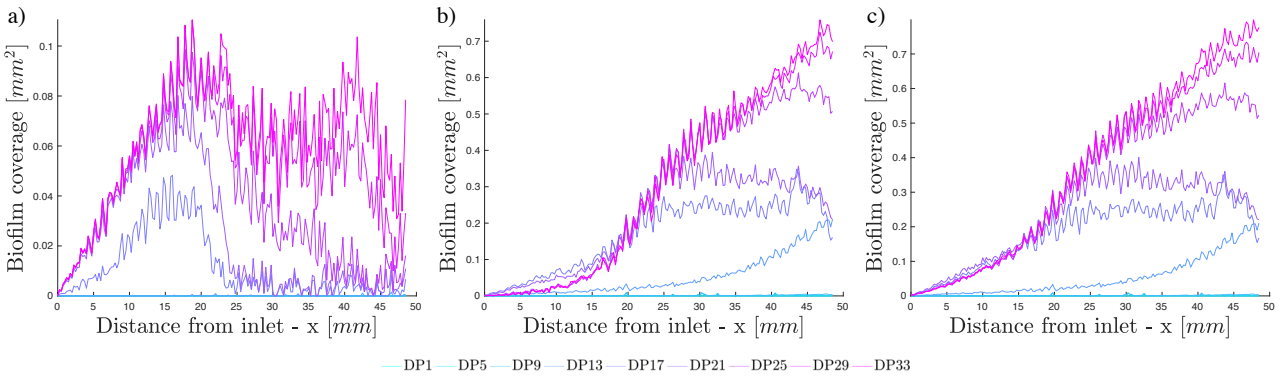

Figure 3.12: Average deposition profile calculated on the three replicates for base biofilm biomass (a), biomass outside the base biofilm structures (b) and total biomass (c), data acquired with strategy 1. The deposition profile are plotted for the acquisition 1, 5, 9, 13, 17, 21, 25, 29, 33.

The average distribution of biomass (taking the average value between the three replicas) as a function of time on a linear and semi-logarithmic scale is shown in figure 3.13. The total biomass (black dots) in our porous system, after the initial exponential growth gets to an intermediate stationary sate that last for about 20 pore volumes and, then, an additional growth phase emerges before a final stationary state is reached around 160 PV. The biomass that is not BB (red dots) seems to control the total biomass (black dots), as they slightly differ. In contrast, the BB dynamics (blue dots) is initially exponential with a slower growth compared to the total biomass and around 80 PV reaches a stationary state with carrying capacity that is slightly less than 15% of the total biomass final carrying capacity.

I fit the observed growth curves with the logistic model eq. (1.18) introduced in chapter #1: it is a model depending on two fitting parameters, the growth rate k and carrying capacity N_∞, whose solution is:

$$N(t) = \frac{N_\infty N_0 e^{k t}}{N_\infty + N_0 (e^{k t} - 1)} \tag{3.1}$$

where N_0 is the initial population $N(t = 0)$. The fitted values are summarized within the table 3.3, the growth rate is reported in [1/min] while the population size and the carrying capacity are reported in arbitrary units.

Table 3.3: Values for the fit function - Strategy 1

Strategy 1	k	N_0	N_∞
Base Biofilm - BB	0.015	0.35	2.30E+05
Other than BB	0.03	3	6.50E+05
Total Biomass	0.03	3	7.30E+05

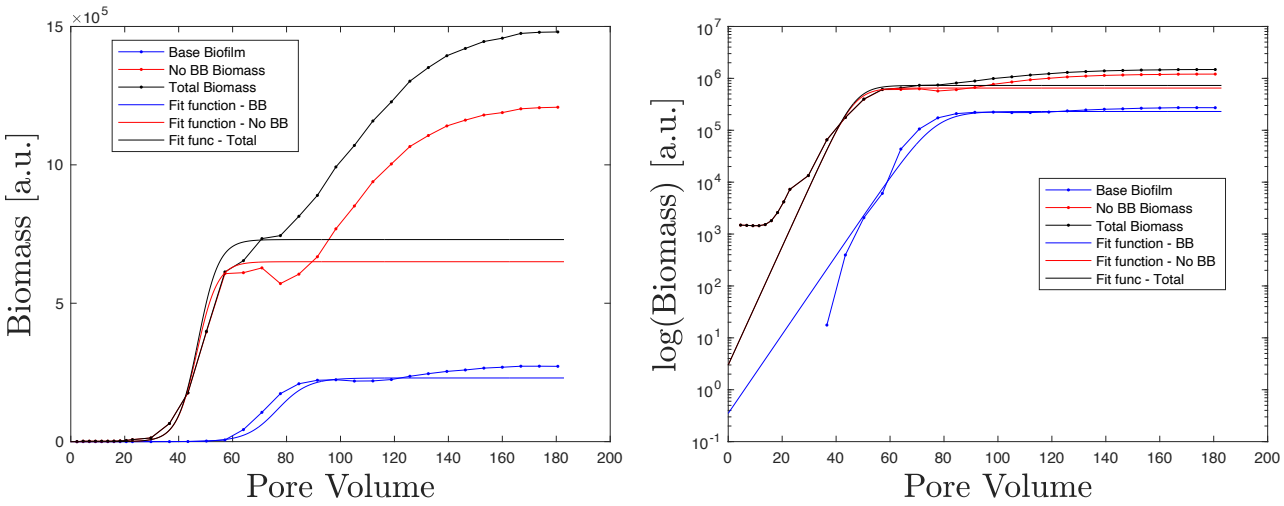

Figure 3.13: Average biomass distribution in linear and semi-logarithmic scale. In both scale are plotted: BB, no BB and total biomass and related fitting function, strategy 1

By computing the outer boundary of the BB-dominated area, as described in the previous chapter,

I computed the maximum distance from the inlet of the BB-area perimeter. The temporal evolution of this location is shown in 3.14, representing how the BB-dominated area advances towards the outlet over time. The results are very similar across the replicas. The BB-dominated area begins to be observed after a few pore volumes are eluted, and its outer boundary develop a parabolic-like shape. The maximum location of the BB-area, the tip of its parabolic perimeter, is initially around 2.5 mm from the inlet and stays constant until it jumps to about 20-25 mm around 2.5 PV, then it seems quite steady for the rest of the experiment. The only significant difference among the replicas is that for replicate 2, the BB-dominated area disappears at time step 27 (corresponding 164 PV).

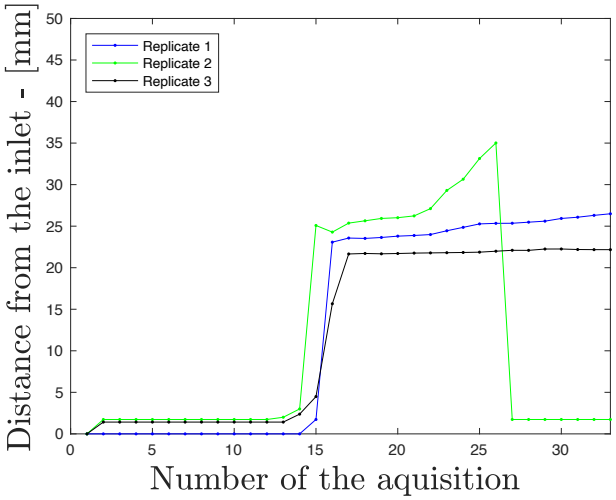

Figure 3.14: Maximal longitudinal length of the BB dominated area for three chip, strategy 1

3.2.2 Strategy 2

As mentioned before the deposition profile and the biomass distribution are calculated and plotted as function of space and time. The architectural differentiation of the biomass was reproducible among all three replicas, as the same phenomena and structures were observed.

Figure 3.15 represents the deposition profile for BB biomass averaged among the three replicas (3.15.a), biomass of everything outside the base biofilm (3.15.b) and total biomass (3.15.c). The BB grows only within the first 15 mm away from the inlet, with a maximum at a distance of 9 mm. The deposition profile, averaged among the three replicas, for the total biomass is not monotonically decreasing as observed for strategy 1: initially, higher near the inlet, later it reaches a maximum after 17/21 acquisitions (corresponding to xxx PV) to decrease towards the outlet. At time xxx PV, the total biomass has two maximum peaks (pink curve in figure 3.15.b), one around 4 mm from the inlet and the second between 18 and 20 mm from the inlet, thus close to the flow outlet. Plotting

the average deposit profile of the base biofilm and comparing it with the average deposit profile of the total biomass, we can see a correlation between base biofilm biomass and total biomass.

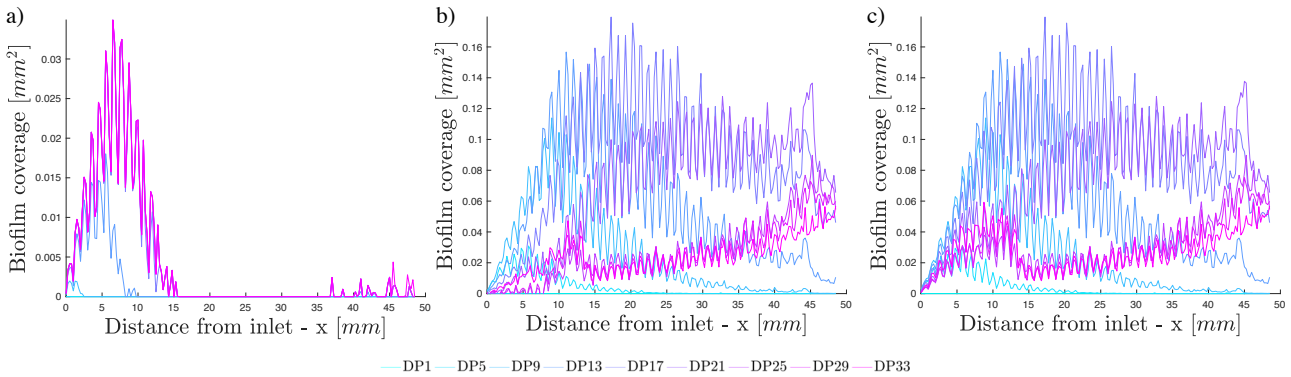

Figure 3.15: Mean deposit profile calculated on the three replicates for base biofilm biomass (a), biomass outside the base biofilm structures (b) and total biomass (c), data acquired with strategy 2. The deposition profile are plotted for the acquisition 1, 5, 9, 13, 17, 21, 25, 29, 33.

The biomass dynamics (considering the average among the three replicas) is shown in figure 3.16, as function of time on a linear and semi-logarithmic scale. As for the injection strategy 1, presented above, we compare the biomass dynamics data with the logistic model, by fitting the growth rates and carrying capacities. The average BB growth exponentially with a lower rate than the non BB and the total biomass. It also reaches a lower carrying capacity when at steady state. The fitted parameters are reported on table 3.2.

$$f(t) = \frac{K f_0 e^{r t}}{K f_0 (e^{r t} - 1)} \tag{3.2}$$

with t a row vector of nt points spaced by intervals equals to $1e^3$, with the values presented with table 3.4.

Table 3.4: Values for fit function - Strategy 2

Strategy 2	r	f0	K
Biomass distribution - BB	0.03	40	7.50E+04
Biomass distribution - no BB	0.06	50	3.50E+05
Biomass distribution - total	0.06	40	4.25E+05

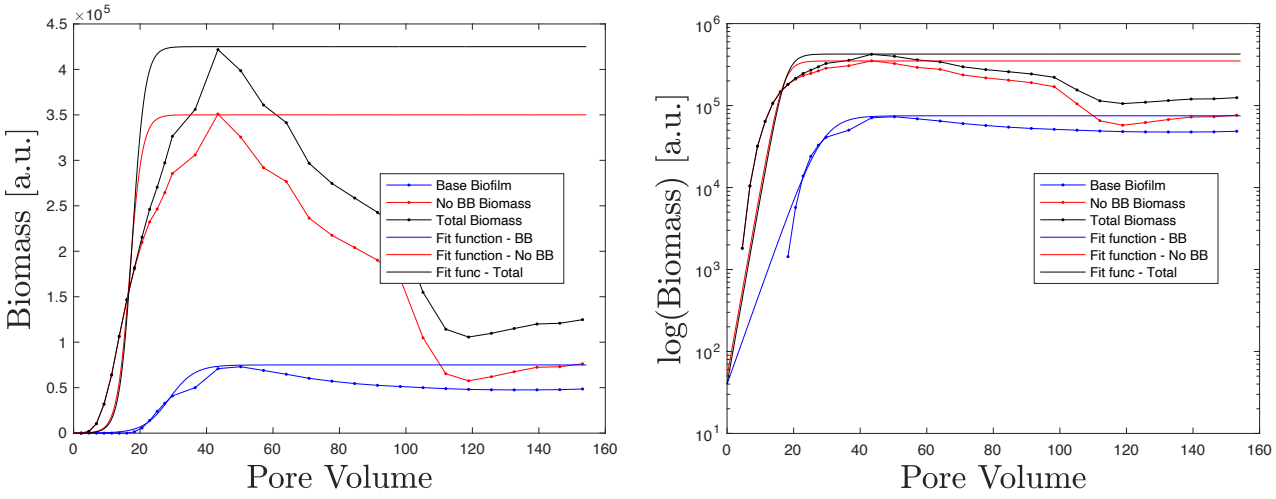

Figure 3.16: Average biomass distribution in linear and semilogic scale. In both scale are plotted: BB, no BB and total biomass and related fitting function, strategy 2.

As for strategy 1, the maximal distance from the inlet was calculated for the BB dominated area (shown in figure 3.17) for each time step and for each channel and plotted as a single point over time. In the following figure it is shown the development of the BB dominated area and the maximum reached longitudinally. For all three channels, the BB dominated area is stationary till the 7th time step, after that it increase till attempt the maximum values between 32.5 and 39 mm, staying constant till the end.

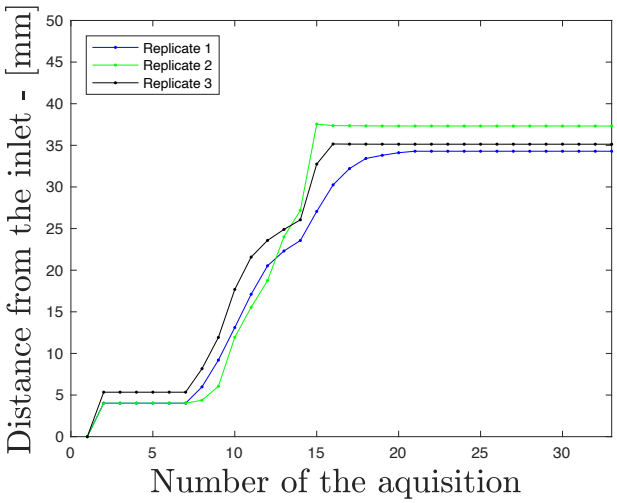

Figure 3.17: Maximal longitudinal length of the BB dominated area for three chip, strategy 2

Chapter 4

Discussion

By studying the growth and development of *P.Putida* bacteria (KT2440 ΔfliM) trough porous media under a controlled flow in a confined space, it is possible to extract deposition profiles and growth curve of biomass distribution over time, through timelapsed images. Qualitative analysis of the data confirmed that in a state without flow and without pores, the bacteria grow steadily, maintaining the same structures homogeneously over the entire surface. In a flow state, however, the architecture of the biomass changes depending on the strategy used. In strategy 1, i.e. during the injection of only a nutrient solution, an initial homogeneous growth was seen on the surface of the porous media, in contrast to strategy 2.

Generally, it can be said that the types of structures displayed in the porous media are the same for the two strategies, however, the timing and respectively the areas inherent to each type of structure change. The structures observed are: base biofilm, ripples, streamer (single or double filament downstream the grains), and, unexpectedly, the formation of a BB dominated area from the inlet towards the middle of the porous channel. This parabola created boundaries inside and outside of which the biomass structured itself in specific ways. The BB dominated area is seen after 54 pore volume for the strategy 1 and after 41 for the strategy 2, despite the fact that for the first 20 pore volume there seemed to be less biomass in strategy 2 than in strategy 1. Comparing the figure 3.14 and the 3.17 it's visible that the BB dominated area appears sooner for the second strategy than the first: for the first strategy it appears at the 15th acquisition, and it stay constant till the end, for strategy 2 it start increasing after 7 time step till achieve the maximum at the 15th acquisition. This difference between the two strategies is the first sign confirming that biomass growth is not constant and is heterogeneous, and also depends on the flow and the elements injected into the system.

Comparing the results obtained through the two different strategies, it can be seen that biofilm coverage reaches higher values for strategy 1. Indeed, looking at the plot shown in figure 4.1, which shows the maximum values reached by the average deposit profiles of the two strategies, we can

see that the average of the deposit profiles for base biofilm of strategy 1 reaches a maximum of 0.11 mm^2 and for total biomass reaches a value of 0.79 mm^2. In contrast, the same values but for strategy 2 correspond to 0.03 mm^2 and 0.20 mm^2. It means that for strategy 1 the total biomass reach a value 7 times higher than the base biofilm biomass, in the same way for strategy 2 total biomass reach maximum value 6.6 time higher than the base biofilm biomass. The average deposition profile for each time step peaks between the first 15-20 mm of the channel decreasing as it moves away from the inlet. However, for strategy 1 after the 21th acquisition the base biofilm are detected on the entire length of the porous channel. Contrary for strategy 2 base biofilm are detected only in the first 15 mm of the channel. It is clear that the strategy 1 has maximum values for deposit profile higher than the strategy 2, meaning that the conditions of growth are better in the first, probably due to the continuous injection of nutrients instead of bacteria. Strategy 2 has a lower biomass because the injected solution consists of nutrients and bacteria, which consume nutrients prior to injection, causing unfavourable or less favourable growth conditions than in strategy 1.

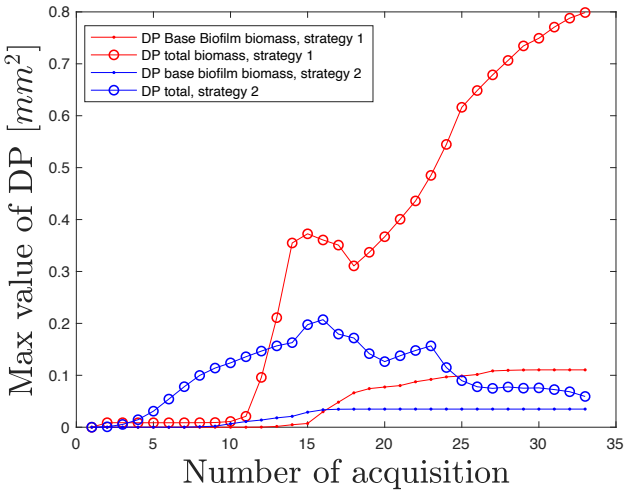

Figure 4.1: Maximum values of the deposit profile extracted from every acquisition for strategy 1 (red) and 2 (blue). The lines with circles represent the maximum value of the deposit profile of total biomass, the lines with dots of the base biofilm biomass.

Comparing the biomass growth over time extracted from the experiments carried out using the two different strategies and plotting the average biomass growth for base biofilm and total for both strategies (figure 4.2), it's clearly visible that the toal biomass for strategy 1 is much higher than strategy 2. Considering the maximum of biomass coverage of base biofilms ($7.09e^4$ nm for strategy 1 and $2.72e^4$ nm for strategy 1) and total ($1.48e^6$ nm and $4.22e^5$ nm), total biomass is 5.4 times higher as base biofilm coverage for strategy 1, and 3.5 higher for strategy 2. Is visible that the total biomass of strategy 2 increase befos as the strategy 1 (after 20 PV versus 40 PV), despite this the total biomass of

the strategy 1 increase 3 time more than the one for strategy 2, and the same is for the base biofilm biomass. As said before this effect is probably due to the difference between the injected solutions.

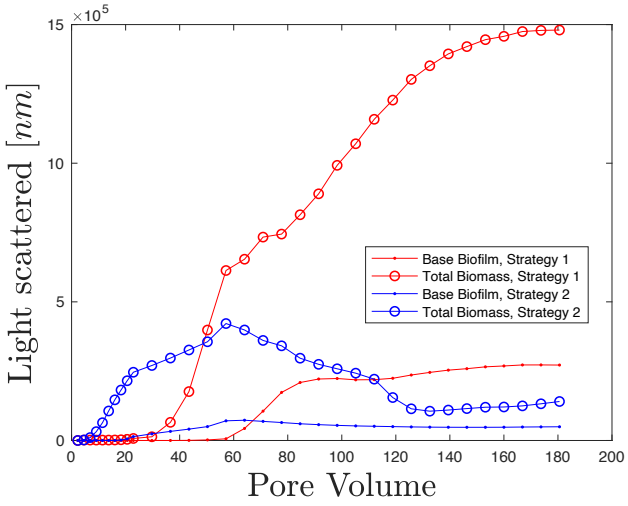

Figure 4.2: Average biomass distribution for both strategies (strategy 1 in red, 2 in blue). The lines with the circles represent the total biomass, the lines with dots only the base biofilm biomass

Thanks to the semi-logical plot fitted with curves (figures 3.13 and 3.16) it is possible to understand the development of biofilm coverage and growth. Starting from the biomass distribution of the strategy 1, it is visible that the total biomass doesn't follow the logistic model. Only the base biofilm biomass follow a logistic model, with an initial exponential growth followed by a stationary state. In fact comparing the qualitative and quantitative data, it is visible that between 50 pore volume and 100, the biomass change structure but it seems like that outside from the BB dominated areathe intensity is higher, this means that after a first phase where the biomass reach a stationary state, then the biomass outside the BB dominated area continues to grown till the 164 pore volume, where the biomass reach a second stationary state. For the strategy 2, the total biomass seems to follow an exponential growth but does not fit the logistic model, as after reaching the maximum it does not continue on the steady state but there is a sudden decrease in the total biomass. In contrast, base biofilm growth would seem to follow the microbial logistic model, in fact after exponential growth it tends to stabilise between $5e^4$ and $7e^4$ nm. For total and base biofilm the initial biomass is higher for the second strategy as the first, and after 40 PV the biomass of the strategy 1 exceed the one of strategy 2. This event can be explained by the difference in the injected solution: in strategy 1 the porous media is saturated with bacteria and a nutrient solution is injected, the bacteria present in the porous system must then quiet the lag phase and stabilise in the new environment and then grow exponentially. In contrast, for strategy 2, the bacteria are in the lag phase in the container of the solution to be injected and once the setup is set up, it takes them 17 pore volume to get into

circulation, but once in the porous media they are already in the exponential growth phase. The discussion of the results shows that the logistic microbiotic growth model is actually not maintained in flow situations through a porous media. The architecture of biofilms is not at all homogeneous at the macroscopic scale, at the pore scale it is, but a function of time and space. In addition the BB dominated area is a clearly exemple of architectural heterogeneity in the way that for the first half of the experiments there is an intense growth followed by a later dispersion of the biomass and the light scattered from it decrease.

The BB dominated area visualised in the experiments for both strategies can be explained as an area where a certain type of growth and architecture is more favourable than outside, base biofilm were only observed inside this area and along its perimeter, whereas outside this area, mainly ripples were observed. Streamers were also only observed within and around the perimeter of the area depending on the weather. This can be explained by the two processes influencing biomass distribution: transport and microbial growth. On the inside and especially on the perimeter of the BB dominated area there are probably conditions favourable to the aggregation of cells and the consequent development of biofilm, and for this base biofilm are visualised; on the outside, on the other hand, the conditions are not favourable to the aggregation of cells and they are transported and accumulated on the surface trough flow as single cells that do not interact with each other, and for this reason they are structured as ripples. In fact the ripples resemble structures visualized in other fields on larger scales, such as for example the transport and accumulation of granular or sandy substances which create accumulations in the shape of dunes, very similar to ripples. The third structure visualized, streamers, are seen in two different forms, as double and single filament, this stricture is still understood because it's not the same for both strategies and not seen outside the BB dominated area. It's understood if they creates thanks to aggregated cells detaching from the base biofilm and transported downstream the grains or if they are structure developing directly downstream the grains.

Chapter 5

Conclusion

The results obtained by studying the growth and development of *P.Putida* bacteria (KT2440 ΔfliM) trough porous media under a controlled flow in a confined space, obtained according to the methods mentioned, have allowed important conclusions to be drawn with regard to the challenges that science has brought to the field of flow-related microbiology in porous media at different scales. Thanks to the microfluidic technique, which has recently been integrated to perform analyses at the microscopic scale, it has been possible to analyse biomass development at the macroscopic but also at the pore scale in transparent porous media. In contrast to the classical theory that carried out analyses in bulk studies focusing on the macroscopic quantities at the inlet and outlet of the porous media, the method adopted in this thesis made it possible to visualise and identify the different processes taking place within the porous media. Using these innovative techniques, the growth and development of biofilms in a porous media was observed, detecting different architectures shaped by the flow of nutrients or bacterial solutions. The structures seen are mainly base biofilm, ripples and streamers, this structures were already mentioned in some papers [19] [17].

All three structures were visualised in specific areas of the porous media, with different timing for the two strategies. The first strategy initially shows a lower total biomass than the second, but then a reversal occurs and strategy 1 has a 3.5 times higher total biomass. The base biofilm, on the other hand, has a biomass 2.6 times higher. How said before the base biofilm biomass follows the logistic growth model with an initial exponential growth, but the total biomass not. This means that the base biomass structures is created thanks to the aggregation of singles cells in sessile communities (biofilm) which continues to grown. The streamers formation stay understood because they're seen inside or along the BB dominated area but are different between the two strategy, it stay understood if they grow thanks to bacterial grow, or if they are aggregated cells detaching from base biofilm and transported by the water downstream the grains. The third structure, ripples, is seen outside the BB dominated area, meaning that the cells accumulated as ripples doesn't have the

same life conditions as the ones inside the area. It's supposed that ripples creation is due to water transport and sedimentation, and the continuous flow of water above the accumulation make the biofilm organize in this special structure.

After this study it can be concluded that the architecture of the biofilm within the porous media is influenced by the flow, by the initial conditions (strategy 1 vs. strategy 2) and also by the injected solution. What was not expected was to see a BB dominated area within the porous media acting as a barrier between the different structures. As the next step in understanding biofilm through porous media will be to understand what is responsible for the creation of this divisive area. First experiments recently conducted show that this area depends on the flow, the amount of injected nutrients but also the presence of oxygen, as the material used for micrfluidics is permeable to oxygen. In order to test the influence of oxygen is necessary to test them trough impermeable materials.

The results confirm that biofilm doesn't grow in an homogeneous way and that the logistic model for microbial growth is not respected inside a porous media. There are many process that controls biofilm transport inside porous system and not only advection and diffusion, how it is for colloids suspension studied by the colloid filtration theory. The physical and biological process as metabolism or interactions between cells (creation of sessile communities) have a lot of importance for the biofilm architecture trough porous media.

Bibliography

[1] Larry W. Mays. *Water Resources Engineering*. John Wiley & Sons, June 2010. Google-Books-ID: Nh8Y3vIjXK8C.

[2] Jacob Bear. *Dynamics of fluids in porous media*. Courier Corporation, 1988.

[3] Zoltán Neufeld and Emilio Hernández-García. *Chemical and biological processes in fluid flows: a dynamical systems approach*. World Scientific, 2009.

[4] C Anthony J Appelo and Dieke Postma. *Geochemistry, groundwater and pollution*. CRC press, 2004.

[5] David A. Stahl David P. Clark Michael T. Madigan, John M. Martinko. Brock Biology of Microorganisms von Michael T. Madigan | Gebraucht | 9780321735515 | World of Books, April 2011.

[6] Malgorzata Peszynska, Anna Trykozko, Gabriel Iltis, Steffen Schlueter, and Dorthe Wildenschild. Biofilm growth in porous media: experiments, computational modeling at the porescale, and upscaling. *Advances in Water Resources*, 95:288–301, 2016.

[7] Lynn W Gelhar, Claire Welty, and Kenneth R Rehfeldt. A critical review of data on field-scale dispersion in aquifers. *Water resources research*, 28(7):1955–1974, 1992.

[8] Peter K Kitanidis. The concept of the dilution index. *Water resources research*, 30(7):2011–2026, 1994.

[9] Marco Dentz, Tanguy Le Borgne, Andreas Englert, and Branko Bijeljic. Mixing, spreading and reaction in heterogeneous media: A brief review. *Journal of contaminant hydrology*, 120:1–17, 2011.

[10] R Allen Freeze and John A Cherry. Groundwater. copyright 1979 by prentice-hall. *Inc., Englewood Cliffs, NJ*, 70632.

[11] Amos Nur, Gary Mavko, Jack Dvorkin, and Doron Galmudi. Critical porosity: A key to relating physical properties to porosity in rocks. *The Leading Edge*, 17(3):357–362, March 1998. Publisher: Society of Exploration Geophysicists.

[12] Pietro de Anna, Bryan Quaife, George Biros, and Ruben Juanes. Prediction of the low-velocity distribution from the pore structure in simple porous media. *Physical Review Fluids*, 2(12):124103, 2017.

[13] Nathalie Tufenkji. Modeling microbial transport in porous media: Traditional approaches and recent developments. *Advances in Water Resources*, 30(6):1455–1469, June 2007.

[14] Timothy R. Ginn, Brian D. Wood, Kirk E. Nelson, Timothy D. Scheibe, Ellyn M. Murphy, and T. Prabhakar Clement. Processes in microbial transport in the natural subsurface. *Advances in Water Resources*, 25(8):1017–1042, August 2002.

[15] Kevin C Marshall. Planktonic versus sessile life of prokaryotes. *The prokaryotes*, 2:3–15, 2006.

[16] Mercedes Berlanga and Ricardo Guerrero. Living together in biofilms: the microbial cell factory and its biotechnological implications. *Microbial cell factories*, 15(1):1–11, 2016.

[17] U. U. Ghosh, H. Ali, R. Ghosh, and A. Kumar. Bacterial streamers as colloidal systems: Five grand challenges. *Journal of Colloid and Interface Science*, 594:265–278, 2021. Publisher: Academic Press Inc.

[18] Shahab Karimifard, Xu Li, Christian Elowsky, and Yusong Li. Modeling the impact of evolving biofilms on flow in porous media inside a microfluidic channel. *Water Research*, 188:116536, January 2021.

[19] David Scheidweiler, Hannes Peter, Paraskevi Pramateftaki, Pietro de Anna, and Tom J. Battin. Unraveling the biophysical underpinnings to the success of multispecies biofilms in porous environments. *The ISME Journal*, 13(7):1700–1710, July 2019. Number: 7 Publisher: Nature Publishing Group.

[20] Giovanni Savorana, Jonasz Słomka, Roman Stocker, Roberto Rusconi, and Eleonora Secchi. A microfluidic platform for characterizing the structure and rheology of biofilm streamers. *Soft Matter*, 2022. Publisher: Royal Society of Chemistry.

[21] Simona Bottero, Tomas Storck, Timo J. Heimovaara, Mark C.M. van Loosdrecht, Michael V. Enzien, and Cristian Picioreanu. Biofilm development and the dynamics of preferential flow

paths in porous media. *Biofouling*, 29(9):1069–1086, October 2013. Publisher: Taylor & Francis _eprint: https://doi.org/10.1080/08927014.2013.828284.

[22] Pablo I. Nikel, Max Chavarría, Esteban Martínez-García, Anne C. Taylor, and Víctor de Lorenzo. Accumulation of inorganic polyphosphate enables stress endurance and catalytic vigour in Pseudomonas putida KT2440. *Microbial Cell Factories*, 12(1):50, May 2013.

[23] Gregory Falkovich. Fluid Mechanics: A Short Course for Physicists, 2018.